Arab J Geosci (2016) 9: 187
DOI 10.1007/s12517-015-2135-6

ORIGINAL PAPER

Rare earth elements and uranium geochemistry in the Al-Kora phosphorite province, Late Cretaceous, northwestern Jordan

Abdulkader M. Abed[1] · **Oday Jaber**[1] · **Mustafa Alkuisi**[1] · **Rushdi Sadaqah**[1]

Received: 18 January 2015 / Accepted: 18 September 2015 / Published online: 10 March 2016
© Saudi Society for Geosciences 2016

Abstract Sixty-three samples representing the phosphorite deposits of the Al-Kora province in northwest Jordan are analyzed for their major and certain trace elements including the rare earth and uranium. They are collected from the following four sections: Tubna, Dair Abu Sa'id, Wadi Al-Arab, and Wadi Ziglab. The samples studied are mainly phosphorite packstone/grainstone consisting of phosphate intraclasts and vertebrate skeletal fragments (bone and teeth) of varying sizes, associated with minor carbonate wackestones. Laminated, in situ phosphorites, sometimes called pristine phosphorites, are also present. The Al-Kora phosphorites are authigenic, i.e., precipitated from the interstitial solutions enriched with the phosphate ion. Carbonate fluorapatite (CFA) or francolite is the dominant mineral. Geochemical data suggest that the analyzed elements can be grouped into (a) land-derived detrital clay group (Al_2O_3, Fe_2O_3, TiO_2, K_2O, Cr, Ga, Hf, Nb, Rb, Th, and Zr). This group constitutes less than 5 % of the total elemental concentrations in the analyzed samples, (b) marine- or seawater-derived phosphate-carbonate group (P_2O_5, CaO, MgO, Na_2O, Ba, Sr, U, Y, and the 14 rare earth element (REE)), making the bulk of the samples studied, and (c) organic matter/detrital clay group (Cr, Ni, Mo, Cu, Pb, As, Zn, and Sb). Uranium substitutes for Ca in the CFA structure with a range from 1 to 186 ppm for all samples including carbonates, with an average of 58.4 ppm. Average for the phosphate-only samples is 101 ppm. The shale-normalized REE patterns exhibit distinct seawater-derived mineral patterns. The patterns are characterized by an enhanced negative Ce anomaly and an enriched heavy REE. This signal (pattern) seems to have survived the phosphogenesis processes. Average Ce anomaly is −0.76, including the carbonate samples. It indicates the fractionation of Ce^{3+} into Ce^{4+} and the deposition of the latter in oxic, or possibly oxygen minimum, seawater. It, thus, confirms the oxic water conditions of the Neo-Tethys Ocean at the time of deposition.

Keywords Phosphorite · Rare earth elements · Ce anomaly · Uranium · Al-Kora · NW Jordan

Introduction

Phosphorites are widespread in Jordan, as part of the Middle East–North Africa–northern South America, and the Caribbean phosphogenic province. Phosphorite deposition was associated with the formation and evolution of the Neo-Tethys Ocean, thus also known as the Tethyan phosphorite province. The Tethyan province accommodates more than half of the phosphorite deposits of the world (Notholt AJ Sheldon and Davidson 1989; Jasinski 2011). Phosphorite deposition throughout this province occurred during the Late Cretaceous-Eocene (Lucas and Prevot-Lucas 1995; Follmi 1996; Van Kauwenbergh 2010; Abed 2013). This is the period when the Neo-Tethys Ocean was an east–west seaway with an active trans-global current circulation (TCC) acting as upwelling currents, necessary for the formation of phosphorites (Follmi 1996; Abed 2013). This highly productive phosphogenic regime came to a halt when the Neo-Tethys Ocean started its final stages of closure because of the continuous northward movement of the Afro-Arabian Plate, its initial subduction beneath the Eurasian Plate, and the final collision with it at around the end of the Eocene (Sharland et al. 2001; Stampfli and Borrel 2002; Powell and Moh'd 2011,

✉ Abdulkader M. Abed
amabed43@gmail.com

[1] Department of Geology, The University of Jordan, Amman 11942, Jordan

2012). In the eastern Mediterranean alone, around 20 billion tons of high-grade phosphorites are concentrated in a relatively small area in western Iraq, NW Saudi Arabia, SE Syria, Jordan, and Palestine (Abed 2013). The majority of these reserves are present in Al-Jalamid in northwestern Saudi Arabi and in the Ga'ara basin in western Iraq (Riddler et al. 1989; Jacobs 1992; Al-Bassam 2007).

Phosphorites in Jordan were discovered early in the twentieth century, and the Jordan Phosphate Mines Company (JPMC) started mining at Ruseifa since 1953. In the 1960s and 1970s, mining started in Al-Hisa and Al-Abyad mines in central Jordan and their deposits are nearly exhausted. In 1988, the Eshidiyya mine was opened after the closure of the Ruseifa mines in the same year (Fig. 1). The future of the phosphorite mining industry in Jordan is concentrated in the Eshidiyya where 1 billion tons of proved reserves are present (JPMC 2013).

On the other hand, Al-Kora phosphorite deposits in northwestern Jordan were discovered in the early 1980s (Mikbel and Abed 1985), where more than 350 million tons of high-grade phosphorites were reported (Fig. 1). Abed and Al-Agha (1989) and Sadaqah (2000) had shown that the phosphorite deposits are present in a wider area than previously mapped by Mikbel and Abed (1985). At the moment, the JPMC is not considering the mining of Al-Kora deposits because the area is highly populated compared with the desert area of Eshidiyya mines and because of transport costs to the Gulf of Aqaba (Fig. 1). However, the Al-Kora deposits remain as future reserves that can be exploited when other resources are depleted.

The aim of this work is to (a) investigate the rare earth element (REE) geochemistry of the Al-Kora phosphorite deposits and (b) study the distribution of uranium in these phosphorites as a response to Jordan's efforts to use nuclear energy as a partial substitute for fossil fuel.

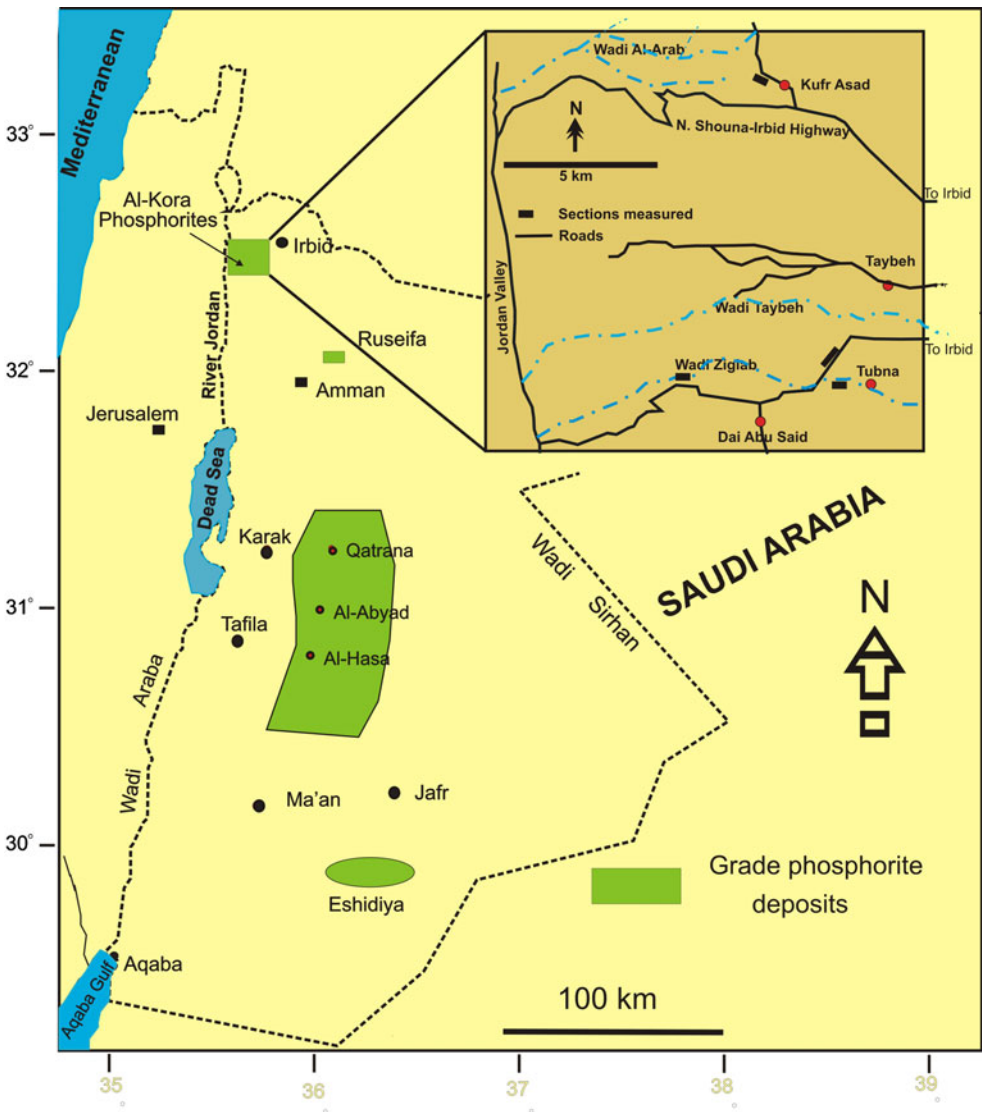

Fig. 1 Location map of the high-grade phosphorites in Jordan. The four sections measured are shown in the inset map (after Abed et al. 2014)

Geological setting

The investigated phosphorites are present in the Al-Kora province, west of Irbid, in the extreme northwestern part of Jordan (Fig. 1). These deposits are far to the north from the conventional phosphorite deposits in central and southern Jordan. They belong to the same formation, Al-Hisa Phosphorite (AHP) Formation or simply Al-Hisa Formation (Powell 1989). The age of the AHP is upper Campanian-lower Maastrichtian (early Maastrichtian (Burdon 1959; Hamam 1977; Abed and Ashour 1987; Capetta et al. 1996) and late Campanian (Bender 1974; Pufahl et al. 2003; Powell and Moh'd 2011)). Table 1 shows the stratigraphic nomenclature of the Belqa Group which includes the AHP. The AHP is divided, in central and southern Jordan, into three formal members, namely, the Sultani Member at the base, the Bahiyya Coquina as the middle member, and the Qatrana Member at the top. The major phosphorite deposits in Jordan are concentrated especially in the upper part of the AHP or the Qatrana Member (Bender 1974; El-Hiyari 1985; Powell 1989; Abed and Sadaqah 1998).

Al-Kora province is folded with varying degrees of intensity, which explains the presence of the outcrops of the AHP within anticline structures such as the Tubna and Dair Abu Sa'id areas. Other outcrops of the AHP are present in deeply cut wadis under the much thicker Muwaqqar Formation overlying the phosphorites such as the deposits of Wadi Al-Arab to the NW of Kufr Asad and in Wadi Ziglab WNW of Dair Abu Sa'id (Fig. 1).

Four sections are measured in this work. They are the Tubna section from a road cut below this village, Dair Abu Sa'id section along the main road leading to Irbid, Wadi Al-Arab section to the northwest of Kufr Asad town, and the Wadi Ziglab section from a deep wadi cut leading to the Ziglab Dam. Figure 1 shows the localities of the four sections, while Fig. 2 shows their lithologies. The thickness of the AHP in the Al-Kora province is less than 10 m. This is a highly reduced thickness compared with the formation thickness in Ruseifa and central Jordan (All-Hisa and Al-Abyad) where it reaches 65 m. One of the reasons for the reduced thickness is the absence of the middle member of the AHP, the Bahiyya Coquina, which could be more than 30 m thick in central Jordan (Abed and Sadaqah 1998). The Bahiyya Coquina consists of oyster buildups or bioherms that can be seen from Ruseifa in the north to the Eshidiyya in the extreme south, thus indicating a drastic difference in the depositional environment of the AHP in Al-Kora compared with these localities (Bender 1974; El-Hiyari 1985; Abed and Sadaqah 1998; Powell and Moh'd 2012).

The highest-grade phosphorite deposits in the Al-Kora province are the uppermost 3 m or so that consist of continuous, friable high-grade deposits. Toward the lower parts of the section, some bedded chert horizons do interfere with the phosphorites.

Methodology

Sixty-three representative samples were collected from the four sections measured. The samples were taken from all the lithologies encountered in the field: limestone, marl, chert, phosphatic limestone and marl, silicified phosphates, and pure

Table 1 Nomenclature of the Cretaceous formations and the stratigraphic position of Al-Hisa Phosphorite Formation and the Muwaqqar Chalk Marl Formation

Age		Group	Formation member	
Tertiary	Eocene	Belqa	Shallala	
			Umm Rijam Chert Limestone	
	Maastrichtian-Paleocene		Muwaqqar Chalk Marl (MCM)	
Late Cretaceous	Maastrichtian		Al-Hisa Phosphorite (AHP)	Qatrana Phosphorite
				Bahiyya Coquina
				Sultani Phosphorite
	Campanian-Santonian		Amman Silicified Limestone	
	Coniacian		Ghudran	Dhiban Chalk
				Tafila
				Mujib chalk
	Turonian	Ajlun	Wadi Es Sir	
			Shueib	
	Cenomanian		Hummar	
			Fuheis	
			Na'ur	
Early Cretaceous	Aptian-Albian	Kurnub (Hathira) Sandstone Group		

Source: (Masri 1963; El-Hiyari 1985)

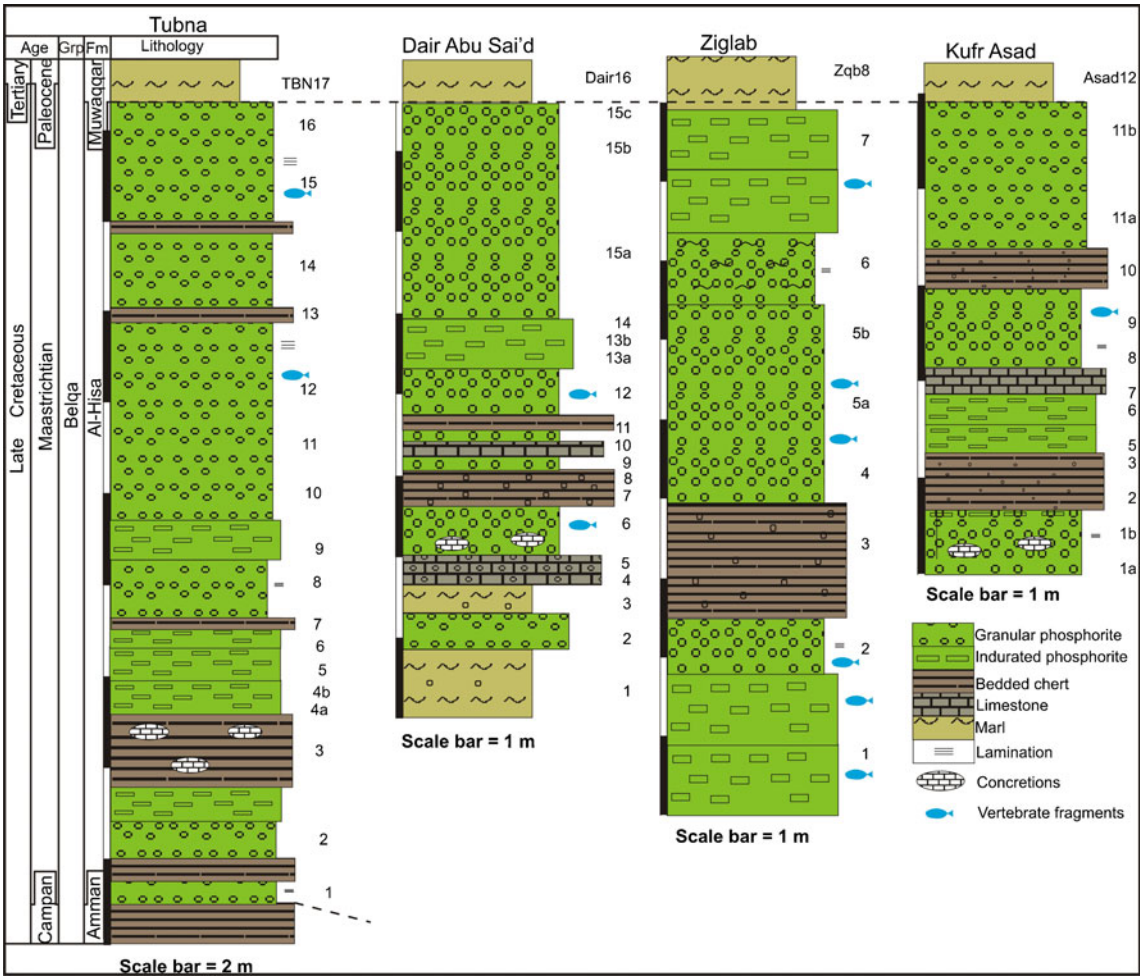

Fig. 2 Lithological logs of the four sections measured. Kufr Asad section is also called Wadi Al-Arab. *Dashed line on top* of the sections is the contact with overlying Al-Hisa Formation

phosphorites. All samples were thin sectioned and stained for petrographic investigation following standard methodology of thin sectioning and staining. Part of each sample was pulverized by means of A Teema mill to pass 200 mesh for mineralogical and chemical analyses. Mineralogical analysis was made by means of an X-ray diffractometer (XRD) on the random powder. All the samples were run using a scanning rate of 2°/min, from 2 to 65° 2θ, range 4×10^3, and a chart speed 2 cm/min on a Philips Xpert MPD housed in the Geology Department, University of Jordan.

Around 20 g of the powder of each sample was sent to ACME Laboratories, Vancouver, Canada, for chemical analysis. The sample powder was fused with lithium metaborate/tetraborate and then digested with nitric acid. The resultant solution was analyzed by inductively coupled plasma ICP-ES-ES for major and trace elements, while the rare earth elements were analyzed by ICP-MS. Some samples were run in duplicates to ensure reproducibility.

Loss on ignition (LOI%) at 550 °C is performed on duplicates of each sample. The powder is weighed in crucibles and then transferred into a furnace for 2 h at 105 °C. The crucibles are then taken to a desiccator to cool down before being weighed to determine the humidity contents of the sample powder. At this stage, the water adsorbed on the clay minerals and other material is removed. The cooled crucibles are then transferred into an oven with 550 °C for 2 h, cooled in a desiccator, and weighed for their organic matter contents. Normally, the differences between the duplicate samples are less than 3 %. The measurement is repeated if the error is more than 5 % (e.g., Abella and Zimmer 2007). Structural water of certain minerals such as the clay minerals especially kaolinite, and other minerals like goethite and gypsum, can cause a serious error to LOI% at 550 °C depending on their abundance in the samples analyzed (e.g., Sun et al. 2009). However, the clay mineral contents in the analyzed samples are too small to affect the use of LOI% at 550 °C as a measure to organic matter. Furthermore, no other minerals with appreciable percentage of structural water, such as gypsum, or goethite are seen in the X-ray diffraction charts of the random sample powder.

Few samples of the high-grade phosphorites were analyzed for their F and CO_3^{2-} contents. Fluorine is analyzed by spectrophotometry where the sample solution is treated with

certain reagent to develop a color. The intensity of the color is proportional to the concentration of F in the sample (e.g., Yamamura et al. 1962; Barghouthi and Amereih 2012). The structural carbonate, CO_3^{2-} residing in the crystal structure of francolite, is calculated by the pair-peak method on the XRD chart (Gulbrandson 1970). It is now well known that CO_3^{2-} substitutes for PO_4^{3-} along the *a* axis (e.g., 410 peak at 51.6° 2θ) but not along the vertical *c* axis (004 peak at 53.1° 2θ) (McClellnn and Lehr 1969; Gulbrandson 1970; McClellan 1980; McClellan and Kauvenbergh 1990). Because the radii of the CO_3^{2-} and PO_4^{3-} ions are not the same, the *d* spacing along the *a* axis is changed while the *d* spacing along the *c* axis is kept constant. Consequently, the angular difference between two XRD peaks is measured on the XRD chart (Δ2θ (004)–(410)) and is used as a measure to the content of CO_3^{2-} in phosphorite samples. The regression between the CO_3^{2} contents and (Δ2θ (004)–(410)) has a standard error in the order of 0.55. Thus, there is no problem with the reproducibility and precision of the CO_3^{2-} contents because of the good control on the measurements of (Δ2θ (004)–(410)) on the XRD charts; however, the accuracy of the pair-peak method is in the order of 10 %.

Results and discussion

Petrography

Petrographic investigation shows that the samples studied consist of a relatively pure phosphorite on one hand and a pure carbonate on the other hand, with intermediate composition of most other samples. The carbonates consist essentially of planktonic foraminifera embedded in a micrite matrix (Fig. 3a). The ratio of tests to micrite is variable, but the sections seen are all wackestones, microfacies type 1 (MF 1). The abundance of both planktonic foraminifera and micrite indicate a basinal or offshore, open marine environment (Flügel 2004).

Phosphate is present with the carbonates to produce phosphatic wackestones (MF 2; Fig. 3b). The latter can grade up to calcareous phosphorite wackestone when the phosphate material becomes dominant (MF 3; Fig. 3c).The particles consist of planktonic foraminifera with similar size, and/or larger, phosphate particles (intraclasts and skeletal fragments) plus in situ, elongated, wavy phosphate mud lamina usually embedded with the micrite lamina (Fig. 3d). This type of

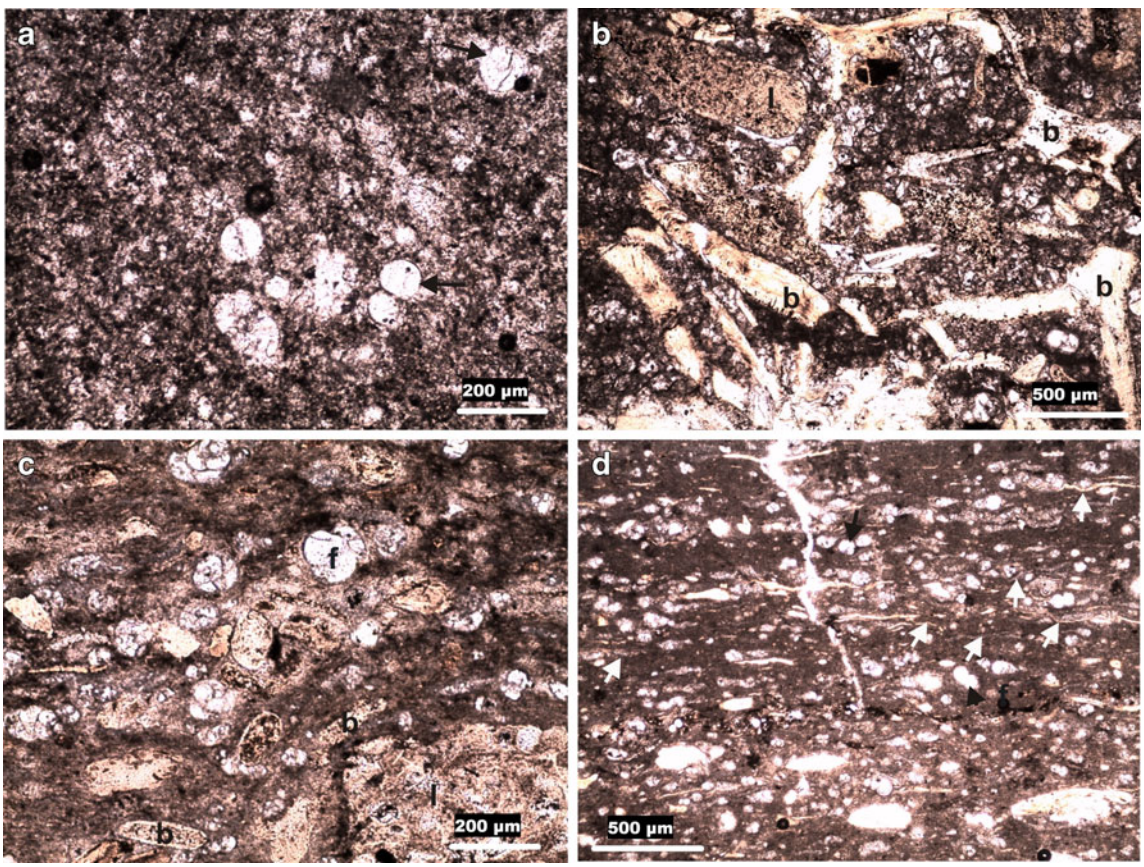

Fig. 3 Petrography. **a** Planktonic foraminifera (*arrows*) in a wackestone with practically no phosphate particles, plane polarized light (PPL). **b** Phosphorite wackestone, *b* bone fragments, *i* phosphate intraclasts in a micrite matrix, PPL. **c** Foraminiferal phosphorite wackestone, *f* foraminifera tests mostly planktonic, *b* bone fragments, *i* phosphate intraclasts in a micrite matrix. **d** In situ phosphate lamina or pristine phosphorite (*white arrows*) in a slightly laminated micrite, with abraded planktonic foraminifera (*black arrow*) and phosphate particles, PPL

laminated phosphorite is called here pristine phosphorite, i.e., not reworked.

True or high-grade phosphorites are represented by phosphorite packstones (MF 4; Fig. 4a) and phosphorite grainstones (MF 5; Fig. 4b). In both microfacies, the phosphate particles consist, predominantly, of phosphate intraclasts of varying sizes and vertebrate skeletal fragments (bones and teeth) in a micrite matrix or calcite cement, respectively. Some foraminiferal tests may be present. Foraminiferal tests are rarely phosphatized. The presence of high accumulations of phosphate particles may be interpreted as due to the reworking of preexisting phosphatic carbonate fancies such as those describe in MF 2 in a relatively shallower marine conditions. The absence or the low percentage of micrite in phosphorite grainstones and packstones can be taken as due to winnowing associated with the reworking process. These two microfacies represent the upper 2–3 m of the four sections investigated and consist of high-grade phosphorite deposits with up 35 % P_2O_5 (see below).

Millimeter-scale lamination is not uncommon in the above-mentioned microfacies. In the typical examples, such as Fig. 4c, a phosphatic carbonate wackestone is alternating with phosphorite packstones/grainstone. Most probably, reworking and winnowing of the former can produce the latter due to slight changes in the environment of deposition.

Quartz, when present, is very angular and most probably of biogenic origin (Fig. 4d). The Al-Kora province is around 400 km to the north of the shorelines of the Neo-Tethys platform. Consequently, transportation of detrital quartz to the study area might be difficult (Powell and Moh'd 2011; Abed 2013). The few samples with high silica contents in the chemical analysis are due to the presence of the biogenic quartz and the partial or complete silicification of few samples. They are present in association with chert beds toward the base of the measured sections.

Mineralogy

The investigated samples consist predominantly of apatite with calcite and minor quartz. Because of the abundance of the carbonate and fluorine in the apatite structure, the apatite species present in the studied samples is carbonate fluorapatite (CFA), also called francolite (Bentor 1980; McClellan and Kauvenbergh 1990).

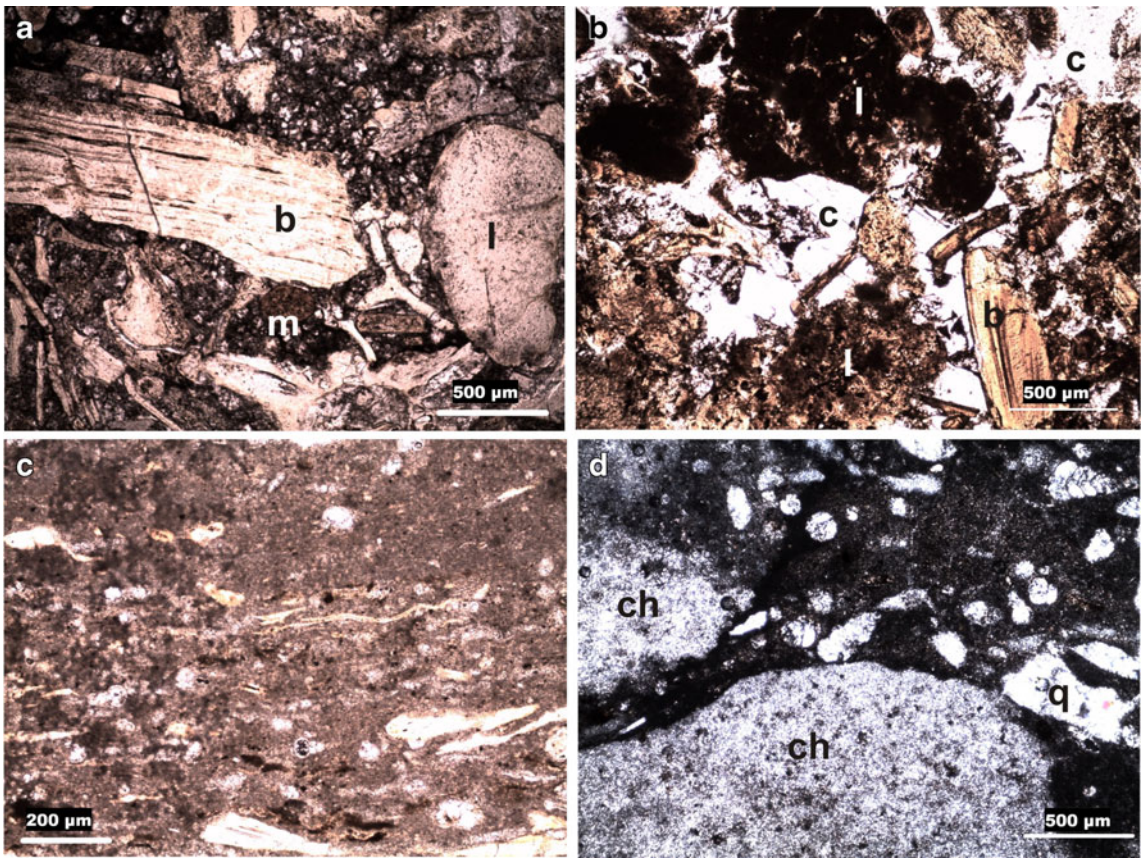

Fig. 4 Petrography continued. **a** Phosphorite packstone, *b* bone fragments, *i* phosphate intraclasts, *m* micrite matrix, PPL. **b** Phosphate grainstone, *b* bone fragments, *i* phosphate intraclasts, *c* calcite cement, PPL. **c** Lamination in some samples showing a micrite lamina with very few phosphate particle (*upper*) and a phosphate lamina (*lower*), PPL. **d** Chert rock fragment (*ch*) and angular quartz (*q*) in few sample with some foraminifera tests in a micrite matrix, XPL

Geochemistry

Thirty-two elements were analyzed in 63 samples from the Al-Kora phosphorite province in northwestern Jordan (Table 2), excluding the REE and Y which are shown in Table 3. Statistical analysis using the correlation coefficient and *R*-mode factor analysis indicates that the analyzed elements are distributed within the following mineralogical phases:

1. **Elements associated with land-derived detrital clay material**

This phase includes the following elements: Al_2O_3, Fe_2O_3, TiO_2, K_2O, Cr, Ga, Hf, Nb, Rb, Th, and Zr. Aluminum is the lead element in this group which is usually taken as indicative of the clay fraction within the sedimentary rocks (Krauskopf and Bird 1995; Brownlow 1996). Table 2 shows that Al_2O_3 has an average of 0.91 % with a minimum of 0.4 and a maximum of 6.45 %. If all the Al_2O_3 is within the detrital clay minerals, and regardless of the type of the clay mineral present, the clay fraction in the samples analyzed will be less than 5 % in average (Weaver and Polland 1975). In other words, the land-derived element forms around 5 % of the samples studied. The three major elements Al_2O_3, Fe_2O_3, and K_2O are present within the crystal structure of the clay minerals depending on the type of the clay minerals (e.g., Weaver and Polland 1975). The TiO_2, Th, and Zr form their own detrital minerals such as tourmaline, thorite, and zircon, respectively. They are transported and deposited with the clay fraction as fine discrete minerals. Niobium (Nb) substitutes for Ti despite the fact that it can, rarely, form its own mineral. Gallium substitutes for Al, Hf substitutes for Zr, and Rb substitutes for K (e.g., Krauskopf and Bird 1995; Brownlow 1996; White 1997). All the above-mentioned elements have a highly significant correlation coefficient with Al_2O_3 and between each others. Figure 5 shows diagrammatically few representative plots between Al_2O_3 and each of Fe_2O_3, Ga and Hf with correlation coefficients more than 0.89, while Fig. 5d is a plot between Zr and Nb with $r=0.85$.

Average SiO_2 content is 16.50 % in all 63 samples and does not correlate positively with Al_2O_3 or any one of elements in the detrital phase discussed above, meaning that the major content of the silica is not associated or accommodated in the detrital clay phase. This average is too large to be accommodated in the less than 5 % detritals. Thin section investigation revealed two types of silica in the studied samples. First, it occurs as a discrete, very angular quartz grains, and in a rare case, chert rock fragments. Both the quartz grains and the chert rock fragment are, most probably, of biogenic origin. The biogenic origin of quartz is indicated by the fact that the quartz grains have a very angular shape throughout the samples investigated. Such highly angular quartz grains cannot be of siliclast origin, transported 400 km from the continent where the shorelines of the Late Cretaceous Tethys Ocean to the south and southeast were located (Powell and Moh'd 2011; Abed 2013). The rare chert rock fragments are most probably derived from the chert interbedded with the phosphorites in the AHP Formation. The biogenic origin of the bedded chert in the Amman and Al-Hisa Phosphorite Formations of Jordan was discussed at length by Abed and Kraishan (1991). The second source of silica is the partial or total silicification of some samples. For example, samples Tbn3 and Tbn5 are completely silicified and have 95.41 and 97.92 SiO_2%, respectively.

2. **Elements associated with the seawater-derived phosphorite-carbonate material**

This phase includes P_2O_5, CaO, MgO, Na_2O, Ba, Sr, U, Y, and the 14 REEs. Figure 6 shows some representative binary plots from this group. P_2O_5 and CaO are the two major elements making the framework of the CFA mineral. However, the low correlation coefficient ($r=0.38$) between the two elements, despite being positively significant, is explained by the presence of substantial amount of calcium also in the carbonates as calcite and dolomite. MgO is present in a very few samples as late diagenetic dolomite rhombs. Na_2O substitutes for calcium in the francolite structure with a significant positive correlation as shown in Fig. 6a (McClellan and Kauvenbergh 1990). Strontium follows Ca in its minerals. Because the CFA crystal structure is more open than the tight calcite structure, the high Sr values (up to 2500 ppm Sr) are accommodated in the CFA not in the calcite as shown in Fig. 6b ($r=0.90$) (Prevot and Lucas 1980; McClellan 1980). Barium forms its own minerals, especially the sulfate and carbonate which are not detected in the samples studied. However, Ba, in the studied samples, is substituting for Ca ($r=0.51$). Ba has a relatively large ion, larger than Sr, and the higher contents of Ba, more than 500 ppm, are most probably accommodated in the CFA structure as shown in Fig. 6c. Uranium, Y ($r=0.47$; Fig. 6d), and the REE substitute for Ca in the CFA structure with a higher positive correlation as discussed below.

3. **Elements associated with total organic matter and the detrital clays**

This phase includes Ni, Mo, Cu, Pb, As, Zn, and V. These elements seem to be adsorbed onto the total organic matter (TOC) and/or the detrital clays or both (e.g., Prevot 1990). Statistical analysis shows that the organic matter has a significant positive correlation with Al_2O_3 ($r=0.54$; Fig. 7a) and the other elements in the detrital phase. This relationship is most probably due to that both constituents, the TOC and the clays, are admixed as a fine-grained matrix in the samples analyzed,

Table 2 Chemical analysis for the major elements (in %) and certain trace elements (in ppm)

	SiO_2	Al_2O_3	Fe_2O_3	MgO	CaO	Na_2O	K_2O	TiO_2	P_2O_5	LOI	Sum	TOC	Cr	Ba	Co	Ga	Hf
Tbn1	4.98	1.56	0.64	0.44	49.61	0.13	0.11	0.07	5.29	36.7	99.59	3.22	573	1399	1.3	3.8	0.5
Tbn2	2.69	0.81	0.29	0.44	51.46	0.39	0.06	0.04	9.00	34.5	99.69	3.70	340	495	0.5	2.0	0.4
Tbn3	95.41	0.10	0.07	0.02	1.77	0.03	0.01	0.01	0.84	1.8	100.01	0.70	17	92	0.3	1.6	0.1
Tbn4a	0.57	0.13	0.04	0.29	54.81	0.19	0.01	0.01	12.76	30.9	99.67	1.40	91	1023	0.2	0.8	0.1
Tbn4b	10.27	0.97	0.36	0.37	47.87	0.10	0.06	0.05	1.83	37.9	99.78	2.20	199	456	0.6	1.7	0.4
Tbn5	0.71	0.21	0.10	0.48	54.32	0.07	0.01	0.01	4.45	39.5	99.82	1.26	58	92	0.4	0.5	0.1
Tbn6	10.42	0.56	0.33	0.45	48.07	0.10	0.04	0.03	5.38	34.3	99.76	2.48	191	296	0.6	1.6	0.3
Tbn7	97.92	0.07	0.04	0.01	1.00	0.01	0.01	0.01	0.48	0.5	100.02	0.33	17	28	0.2	1.3	0.1
Tbn8	2.98	0.76	0.24	0.39	51.56	0.33	0.04	0.03	8.74	34.6	99.69	4.20	149	449	0.4	1.7	0.2
Tbn9	1.32	0.17	0.08	4.73	48.98	0.19	0.01	0.01	12.84	31.3	99.62	1.72	66	313	0.3	0.4	0.1
Tbn10	1.15	0.17	0.08	0.33	53.27	0.60	0.01	0.01	20.50	23.5	99.64	2.34	75	138	0.8	0.4	0.2
Tbn11	13.52	0.28	0.10	0.22	45.92	0.77	0.02	0.01	27.72	10.9	99.48	2.49	116	1715	0.3	0.3	0.2
Tbn12	26.58	1.16	0.44	0.45	38.11	0.34	0.07	0.04	9.52	23.0	99.78	3.84	241	119	0.4	1.7	0.3
Tbn13	40.76	0.10	0.05	0.21	31.78	0.43	0.01	0.01	20.63	5.7	99.68	1.93	42	323	0.3	0.4	0.1
Tbn14	3.20	0.20	0.10	0.30	52.75	0.49	0.02	0.01	34.66	7.4	99.16	2.15	100	3929	0.7	0.3	0.2
Tbn15a	7.17	0.86	0.39	0.32	49.45	0.47	0.06	0.04	31.81	8.8	99.37	3.25	232	2063	2.2	1.2	0.2
Tbn15b	11.09	0.82	0.24	0.42	47.96	0.25	0.04	0.03	18.63	20.2	99.68	2.80	100	170	0.9	0.6	0.2
Tbn16a	24.29	6.45	3.31	0.79	32.30	0.34	0.44	0.29	20.75	10.1	99.24	5.39	1129	2373	5.7	7.2	2.1
Tbn16b	7.74	2.41	1.47	0.36	47.57	0.25	0.14	0.10	32.59	6.5	99.20	2.60	307	4005	3.3	2.1	0.7
Tbn17	13.29	4.20	2.12	0.37	41.79	0.11	0.23	0.17	2.54	34.8	99.71	0.05	623	115	2.3	3.2	0.8
Deir1	2.15	0.20	0.07	16.65	34.10	0.12	0.02	0.01	1.93	44.3	99.57	2.68	58	297	3.1	0.4	0.1
Deir2	6.54	0.31	0.15	0.17	51.56	0.40	0.02	0.01	33.18	7.2	99.54	2.89	149	109	0.2	0.5	0.2
Deir3	31.63	3.51	1.17	0.74	32.56	0.22	0.25	0.13	15.87	13.4	99.55	5.41	506	189	5.5	4.2	0.6
Deir4	3.92	0.79	0.27	12.58	37.86	0.13	0.04	0.03	8.64	35.3	99.58	2.53	100	51	0.8	0.2	0.2
Deir5	76.38	1.37	0.33	0.19	11.01	0.09	0.11	0.05	1.93	8.4	99.90	2.14	116	44	6.8	1.1	0.4
Deir6	1.45	0.13	0.08	3.29	50.66	0.35	0.01	0.01	25.69	17.5	99.20	2.67	42	3740	0.3	0.3	0.1
Deir7	55.61	0.13	0.04	0.10	24.09	0.25	0.01	0.01	14.99	4.5	99.77	2.03	25	90	10.2	0.4	0.1
Deir8	1.54	0.15	0.09	0.21	53.76	0.47	0.02	0.01	35.24	8.1	99.55	2.78	58	404	0.2	0.3	0.1
Deir9	0.79	0.11	0.06	3.13	51.76	0.06	0.01	0.01	2.82	41.0	99.74	1.41	25	697	1.4	0.4	0.1
Deir10	1.75	0.41	0.18	11.86	40.27	0.19	0.04	0.02	12.67	32.2	99.57	3.05	108	50	0.7	0.3	0.1
Deir11	67.81	0.15	0.04	0.08	17.22	0.20	0.02	0.01	10.72	3.6	99.81	1.38	33	213	18.9	0.3	0.1
Deir12	16.57	0.08	0.04	0.18	45.76	0.36	0.01	0.01	23.70	12.9	99.67	2.40	58	291	5.3	0.2	0.1
Deir13a	0.51	0.04	0.04	0.21	55.17	0.40	0.02	0.01	26.99	16.3	99.63	2.88	50	85	1.4	0.4	0.1
Deir13b	0.79	0.26	0.06	0.40	54.97	0.02	0.01	0.01	1.04	42.4	99.91	0.76	17	15	1.5	0.4	0.1
Deir14	4.06	1.23	0.42	12.07	38.78	0.15	0.07	0.05	9.52	33.2	99.60	2.29	141	42	0.6	1.4	0.3
Deir15a	1.46	0.24	0.18	0.23	53.86	0.38	0.03	0.01	23.66	19.2	99.32	2.53	149	3003	0.6	0.4	0.2
Deir15b	6.99	0.83	0.28	0.25	50.42	0.33	0.13	0.05	9.99	30.4	99.70	3.17	349	352	0.8	0.6	0.7
Deir15c	11.69	4.11	2.00	1.52	37.58	0.57	0.25	0.17	2.19	39.6	99.76	18.40	432	47	5.2	3.8	0.8
Deir16	3.23	0.68	0.36	0.43	52.63	0.31	0.05	0.03	17.15	24.8	99.65	3.09	199	228	2.0	0.5	0.3
Asad 1a	41.13	2.58	0.90	0.70	23.18	0.97	0.15	0.10	6.61	23.4	99.71	13.64	25	127	1.8	3.7	0.5
Asad 1b	7.85	0.21	0.04	0.50	48.00	0.59	0.01	0.01	0.47	42.2	99.88	3.44	25	26	0.2	0.3	0.1
Asad 2	24.95	0.29	0.09	0.24	41.12	0.38	0.02	0.01	17.84	14.7	99.68	1.51	58	219	0.4	0.4	0.2
Asad 3	42.39	1.79	0.63	0.79	26.28	1.29	0.11	0.08	10.11	16.2	99.69	10.40	206	157	0.7	2.5	0.5
Asad 5a	3.64	0.24	0.07	0.39	51.75	0.82	0.02	0.01	24.58	18.1	99.58	3.36	91	216	0.2	0.4	0.1
Asad 5b	3.75	0.07	0.05	0.22	52.71	0.40	0.01	0.01	28.50	13.9	99.57	1.83	75	220	0.2	0.4	0.1
Asad 6	5.34	0.48	0.16	0.57	51.55	0.27	0.04	0.02	8.17	33.2	99.80	1.73	91	64	0.6	0.3	0.2
Asad 7	16.30	1.30	0.48	0.38	43.73	0.46	0.10	0.06	12.35	24.5	99.64	6.26	257	107	0.5	1.5	0.3
Asad 8a	5.33	0.22	0.07	0.44	51.92	0.60	0.01	0.01	21.56	19.5	99.66	3.07	83	363	0.3	0.4	0.2
Asad 8b	3.15	0.14	0.07	0.60	51.91	0.69	0.02	0.01	18.69	24.2	99.51	3.04	58	1997	0.6	0.3	0.1
Asad 9	18.23	0.06	0.07	0.40	45.39	0.35	0.01	0.01	12.88	22.3	99.70	1.43	50	623	0.3	0.4	0.1
Asad 10	10.31	2.26	0.98	0.74	44.28	1.42	0.13	0.09	12.79	26.5	99.53	10.31	307	652	1.4	2.5	0.7
Asad 11a	4.89	0.89	0.45	0.32	51.39	0.39	0.07	0.04	11.14	30.0	99.65	2.46	307	321	0.7	0.3	0.6
Asad 11b	3.20	0.57	0.16	0.34	52.55	0.31	0.05	0.03	9.22	33.3	99.70	2.64	199	168	0.7	0.4	0.3
Asad 12	7.42	1.24	0.40	0.37	47.89	0.48	0.11	0.06	3.50	38.2	99.74	5.75	374	54	0.4	0.4	0.6
Zqb 1	8.29	0.49	0.15	0.18	50.67	0.20	0.03	0.02	20.11	19.6	99.73	2.09	141	117	0.2	0.3	0.2
Zqb 2	42.65	1.85	0.59	0.31	29.51	0.15	0.13	0.06	7.74	16.8	99.79	3.00	241	123	0.8	1.1	0.4
Zqb 3	50.67	1.63	0.65	0.26	24.74	0.18	0.15	0.08	6.86	14.5	99.76	2.48	241	154	0.9	2.1	0.3
Zqb 4	10.09	0.14	0.06	0.20	49.32	0.40	0.02	0.01	24.28	15.1	99.63	2.20	75	259	0.2	0.4	0.1
Zqb 5a	37.09	0.08	0.05	0.12	34.37	0.28	0.01	0.01	21.49	6.2	99.74	1.73	58	233	0.2	0.3	0.1
Zqb 5b	2.97	0.19	0.08	0.22	53.15	0.34	0.01	0.01	25.21	17.5	99.65	2.33	75	279	0.2	0.3	0.2
Zqb 6	32.12	1.19	0.38	0.31	35.80	0.28	0.09	0.05	15.13	14.4	99.74	2.24	158	204	0.4	0.6	0.8
Zqb 7	1.07	0.12	0.05	6.33	47.16	0.26	0.01	0.01	16.87	27.6	99.51	2.39	100	899	0.2	0.4	0.1
Zqb 8	3.05	0.66	0.14	0.33	52.76	0.10	0.06	0.03	3.20	39.4	99.81	2.28	191	98	0.2	0.3	0.4

	Nb	Rb	Sr	Th	U	V	Zr	Mo	Cu	Pb	Zn	Ni	As	Cd	Sb
Tbn1	1.3	4.4	1024.6	0.9	33.2	373	29.5	6.9	78.3	9.9	200	45.1	14.2	33.0	4.0
Tbn2	0.5	2.4	1296.0	0.6	37.2	160	19.6	1.8	64.2	4.5	177	37.4	8.6	28.2	1.7
Tbn3	1.2	0.2	69.1	0.2	5.7	13	7.1	0.8	10.4	0.4	17	5.3	1.2	0.4	0.3

Table 2 (continued)

	Nb	Rb	Sr	Th	U	V	Zr	Mo	Cu	Pb	Zn	Ni	As	Cd	Sb
Tbn4a	0.3	0.4	1377.0	0.2	48.6	60	15.0	0.5	35.6	0.9	46	7.1	3.8	8.1	0.4
Tbn4b	0.7	2.3	742.5	0.5	13.7	183	16.4	4.9	33.6	2.7	226	44.6	9.7	27.7	1.7
Tbn5	0.1	0.4	1014.5	0.2	17.0	60	6.0	1.0	23.5	0.8	104	15.7	1.7	9.6	0.5
Tbn6	0.2	1.6	1035.8	0.4	26.1	154	13.6	3.1	54.7	2.7	227	51.1	9.1	37.4	3.7
Tbn7	0.7	0.1	41.7	0.2	5.6	17	1.3	0.8	3.7	0.2	13	3.9	0.9	0.3	0.3
Tbn8	0.5	2.0	1252.9	0.4	99.9	126	13.7	4.4	26.4	2.2	364	50.5	4.8	36.9	1.0
Tbn9	0.1	0.3	1201.2	0.4	104.7	57	8.1	1.0	13.7	0.6	505	48.2	1.2	38.7	0.5
Tbn10	0.1	0.4	1704.6	0.9	73.1	46	10.6	1.2	13.6	0.8	619	52.0	2.8	27.5	0.4
Tbn11	0.1	0.7	2119.2	0.9	103.7	65	13.1	1.6	26.8	1.3	151	20.2	3.3	15.8	0.4
Tbn12	0.4	2.5	1145.3	0.5	35.9	163	13.1	7.1	41.5	3.8	191	59.9	8.3	71.5	2.0
Tbn13	0.1	0.1	1986.4	0.4	83.8	67	7.5	1.6	18.5	1.3	233	14.0	1.6	4.1	0.5
Tbn14	0.1	0.6	2711.2	0.6	116.6	134	12.3	2.4	31.9	1.7	170	23.3	4.4	1.5	0.6
Tbn15a	0.5	2.6	2531.0	0.7	110.4	248	19.2	4.1	42.4	2.4	202	63.9	11.0	3.6	1.9
Tbn15b	0.2	1.7	1599.1	0.7	59.7	157	12.2	2.0	16.9	1.5	314	63.9	7.4	29.1	1.2
Tbn16a	4.4	18.1	1968.8	4.3	164.9	264	97.6	20.9	265.9	6.6	638	420.7	54.4	0.4	6.7
Tbn16b	1.4	4.8	1944.7	1.6	186.8	134	39.0	11.3	66.2	3.8	207	199.3	44.6	0.1	3.8
Tbn17	2.5	9.5	1481.6	2.0	27.1	151	34.0	46.4	120.3	5.4	246	157.3	31.1	1.8	1.5
Deir1	0.1	0.7	637.6	0.2	8.2	102	4.4	2.1	5.6	0.4	115	14.9	0.5	16.1	0.3
Deir2	0.3	0.9	2511.0	1.3	140.6	104	14.7	12.4	31.2	1.5	448	37.3	6.3	43.8	1.2
Deir3	1.8	10.4	1294.7	1.6	66.3	822	32.9	41.2	106.7	8.5	743	139.4	20.0	65.6	3.5
Deir4	0.2	1.9	982.0	0.5	32.6	262	10.4	12.5	17.4	1.1	209	33.5	3.2	32.3	0.8
Deir5	0.8	4.0	268.2	0.5	10.1	198	13.5	12.6	31.7	2.1	194	48.9	0.5	26.4	2.1
Deir6	0.1	0.1	2151.1	0.3	78.7	116	8.9	5.2	14.2	0.7	209	19.5	1.7	19.4	0.5
Deir7	0.1	0.1	1343.8	0.2	54.0	48	6.5	3.1	10.8	0.8	178	16.0	0.5	11.9	0.4
Deir8	0.1	0.3	2555.2	0.2	117.4	111	9.4	6.6	19.0	1.2	276	24.2	1.8	15.4	0.6
Deir9	0.1	0.3	834.4	0.2	8.3	112	2.1	1.7	4.6	0.2	45	7.6	0.5	23.2	0.1
Deir10	0.1	2.0	1320.0	0.3	36.6	222	8.0	4.6	15.1	1.0	151	27.5	2.3	14.3	0.7
Deir11	0.1	0.2	910.5	0.2	34.2	36	6.3	2.3	9.7	0.4	108	8.3	0.5	7.4	0.3
Deir12	0.1	0.2	1989.3	0.3	70.3	96	7.6	2.9	15.8	0.9	142	14.0	1.4	14.2	0.3
Deir13a	0.1	0.1	2468.7	0.2	82.6	120	7.6	2.7	13.7	0.6	147	11.9	2.0	15.4	0.3
Deir13b	0.1	0.2	471.8	0.2	5.1	114	1.1	3.6	2.9	0.3	31	6.2	0.5	51.9	0.2
Deir14	1.0	3.0	969.2	0.6	26.4	311	13.0	20.2	18.1	1.2	122	50.6	9.4	11.5	1.6
Deir15a	0.1	0.9	2222.5	0.9	109.6	89	19.4	8.1	23.6	0.8	72	27.6	6.4	7.0	1.1
Deir15b	0.7	3.4	1612.4	1.0	55.1	54	33.2	2.5	88.2	1.1	80	58.4	6.2	1.2	0.7
Deir15c	2.8	9.6	1063.1	2.1	26.3	89	32.0	19.0	70.5	2.4	226	200.0	36.8	1.0	2.0
Deir16	0.4	1.5	2020.4	1.0	105.0	86	20.5	7.8	43.2	0.9	70	44.7	11.3	2.5	0.9
Asad 1a	1.5	6.3	948.0	1.0	28.2	495	22.7	40.6	54.4	4.5	418	84.4	17.7	50.9	2.9
Asad 1b	0.1	0.2	535.9	0.2	1.6	57	1.9	1.8	5.5	0.2	151	9.0	1.8	32.0	0.2
Asad 2	0.2	0.4	1811.3	0.6	67.0	109	13.1	4.5	15.2	0.8	223	15.8	7.5	23.2	0.9
Asad 3	1.5	4.3	1288.9	1.0	42.1	395	20.5	43.9	42.2	3.0	328	75.5	17.8	20.6	2.8
Asad 5a	0.2	0.5	2612.7	0.5	84.5	132	11.7	4.0	14.6	1.1	185	14.8	6.3	12.9	0.5
Asad 5b	0.1	0.1	2622.5	0.3	88.5	106	11.5	5.1	17.6	0.9	258	16.8	11.0	9.8	0.9
Asad 6	0.3	1.4	1108.3	0.2	22.0	93	9.0	7.7	16.3	1.0	136	28.2	7.0	33.7	0.5
Asad 7	0.9	4.6	1656.1	0.8	39.9	234	19.5	24.9	44.7	2.8	328	68.4	12.9	26.3	1.3
Asad 8a	0.1	0.4	1954.0	0.2	61.3	90	10.9	3.3	13.2	0.9	102	10.3	5.5	13.2	0.4
Asad 8b	0.1	0.4	1745.1	0.2	53.5	89	8.9	2.9	12.8	0.9	87	7.6	6.1	15.9	0.4
Asad 9	0.1	0.1	1483.5	0.2	35.2	78	6.8	2.1	8.7	0.4	118	6.0	3.8	16.8	0.2
Asad 10	1.6	6.5	1339.6	1.0	53.9	448	29.8	9.1	58.1	3.3	669	201.6	27.7	26.4	4.4
Asad 11a	0.5	3.1	1725.6	1.0	61.7	145	29.1	4.1	52.0	1.0	185	65.8	19.2	15.9	1.0
Asad 11b	0.4	2.1	1707.5	0.6	47.5	74	17.8	1.6	47.6	0.6	100	35.0	4.4	7.2	0.6
Asad 12	0.9	4.9	1399.8	1.0	36.6	105	29.7	6.1	85.6	1.5	211	73.8	9.4	11.9	1.4
Zqb 1	0.2	1.0	1475.8	0.7	74.1	93	14.5	5.9	23.3	1.1	150	19.2	6.7	35.3	0.7
Zqb 2	1.1	4.7	747.0	0.9	28.8	306	19.2	27.8	36.1	2.7	250	48.4	14.6	27.1	1.5
Zqb 3	1.5	4.1	694.8	0.8	31.2	539	16.8	25.3	49.4	3.4	365	79.7	20.2	21.9	2.2

Table 2 (continued)

	Nb	Rb	Sr	Th	U	V	Zr	Mo	Cu	Pb	Zn	Ni	As	Cd	Sb
Zqb 4	0.1	0.3	1997.8	0.5	105.3	161	10.8	1.8	13.1	1.0	234	7.9	7.7	16.6	0.4
Zqb 5a	0.3	0.1	1556.3	0.4	72.7	76	9.8	2.4	12.9	0.7	165	10.8	7.7	5.5	0.6
Zqb 5b	0.6	0.4	2021.2	0.4	86.2	174	12.9	2.9	22.3	0.7	149	12.7	10.2	12.1	0.8
Zqb 6	2.5	2.8	1213.8	0.9	49.8	229	36.1	17.7	25.2	1.4	219	56.1	19.6	25.2	2.1
Zqb 7	0.1	0.3	1787.1	0.4	64.7	106	10.3	2.5	14.7	0.6	165	35.3	5.1	9.8	0.7
Zqb 8	0.5	2.1	1069.2	0.6	22.9	29	19.8	1.3	43.7	0.8	83	43.2	4.9	0.8	0.6

and consequently, they behave similarly. However, the relationship between these elements and the TOC is weaker than with the detrital clays. This is indicated by a lower, but still significant, correlation coefficients with the TOC ranging from 0.31 to 0.48, e.g., *r* between TOC and each of Ni, Mo, Cu, Pb, As, Zn, and V are 0.48, 0.47, 0.31, 0.33, 0.48, 0.40, and 0.41, respectively. As an example, As is plotted in Fig. 7c. The range of *r* between these elements and the detrital clays varies between 0.54 and 0.92, e.g., with Ni (Fig. 7b). In both cases, all the correlation coefficients are statistically significant. The remaining parts in Fig. 7 show some representative binary plots, indicating the interrelationships among these elements such as Pb and Cu ($r=0.71$; Fig. 7d), Zn and Cd ($r=0.41$; Fig. 7e), and V and Mo ($r=0.0.71$; Fig. 7f).

All said above, the lower correlation coefficients of these elements with the TOC/clay fraction, mentioned above, might be due to the fact that this group of elements can also be present in the CFA structure. Al-Kuisi M Abed AM Mashal K and Saffarini (2015), while studying groundwater pollution in northwestern Jordan, showed that Mo as MO_4^{2-} substitutes for PO_4^{3-} in the CFA of the phosphorite deposits of the Al-Kora province. They connected the high Mo concentrations in groundwater with the phosphorites deposits. Abed et al. (2014) explained the high concentration of V in the Eshidiyya phosphorites in southern Jordan through the substitution of VO_4^{3-} for PO_4^{3-} in the CFA structure (Nathan 1984; Mckelvey et al. 1986). Al-Kuisi M Abed AM Mashal K and Saffarini (2015) had demonstrated the presence of a positive relationship between As and the phosphorite deposits in groundwater throughout Jordan. Altschuler (1980) had also demonstrated that Zn is enriched in the CFA more than twice its presence in shale as due to substitution with Ca. Cadmium is known to substitute for Ca, and the commercial quality of the phosphorite deposits depends on the levels of Cd (e.g., Altschuler 1980; Prevot 1990). The low and not significant correlation coefficients between all these elements and P_2O_5 may be explained by the abundance of TOC which has mimicked their relationship with the CFA.

Uranium distribution and geochemistry

Uranium replaces Ca in the apatite structure in hexavalent coordination, while calcite does not allow much U to replace Ca due to its lower coordination in the calcite crystal structure compared to apatite (McClellan 1980; Slansky 1986). Correlation coefficient (*r*) with P_2O_5 is 0.86 for the 63 samples analyzed (Fig. 8); *r* is still significant with CaO but much lower, 0.34, because of its being present also in calcite. It seems that there is no relationship with the total organic matter and uranium as indicated by a low, not significant correlation ($r=-0.04$).

Sadaqah (2000) reported relatively higher values for U in the Al-Kora phosphorites, especially in Kufr Asad section. Some of the his results are in excess of 300 ppm U. Table 4 compares the U contents in the major phosphorite deposits in Jordan. The low average of the Al-Kora province is certainly due to the inclusion of almost pure carbonates in the samples analyzed, attested by the CaO and P_2O_5% in Table 2. The average of the phosphorite samples with more 19.5 % P_2O5 (equals around 50 % francolite) is 101 ppm. The latter average lies within the range of the other high-grade Jordanian phosphorites (e.g., Abed 2011)

REEs

Total REE (∑REE), in the analyzed samples, ranges between 1.83 and 240.49 ppm with an average of 44.57 ppm. The lower ∑REE is in carbonate samples with around 1 % P_2O_5, while the higher total is for the true phosphorites with more than 19.5 % P_2O_5. The ∑REE is too low for any economic value of the Al-Kora phosphorite deposits. However, the analysis of the REE gives insight on the provenance and depositional environment of the studied material.

Bedded phosphorites are well known of being of marine origin (e.g., Bentor 1980). Marine sediments, with regard to REE behavior, can be divided into two types. First is the terrestrial or land-derived particulate matter carried to the sea in suspension. This type of material carries the original signature of the REE pattern of the land source with no appreciable fractionation within the 14 REEs. Consequently, the REE pattern would be rather similar to that of shale, i.e., flat patterns (e.g., Piper 1974; Sholkovitz et al. 1994; Piper and Bau 2013). Second is the sediment derived from the dissolved load to the sea which suffers fractionation in oxidized seawater. For example, cerium (Ce), in particular, is oxidized from the soluble Ce^{3+} to the highly insoluble Ce^{4+}, which is

Table 3 Chemical analysis for the rare earth elements, yttrium (in ppm), and the Ce anomaly

NASC	Y	31.1 La	66.7 Ce	7.7 Pr	27.4 Nd	5.59 Sm	1.18 Eu	4.9 Gd	1.02 Ho	2.84 Er	0.48 Tm	3.06 Yb	0.46 Lu	Ce anomaly
Tbn1	33.6	11.3	8.6	2.01	8.5	1.77	0.41	2.44	0.73	2.31	0.36	2.16	0.38	−0.72
Tbn2	42.7	14.2	7.4	2.06	9.3	1.89	0.47	2.69	0.78	2.66	0.41	2.65	0.47	−0.86
Tbn3	3.1	1.2	0.8	0.15	0.5	0.13	0.03	0.22	0.05	0.17	0.03	0.18	0.03	−0.68
Tbn4a	44.4	13.1	6.0	1.63	7.4	1.43	0.35	2.36	0.70	2.26	0.39	2.45	0.46	−0.89
Tbn4b	14.3	5.3	4.5	0.93	3.8	0.82	0.19	1.10	0.28	0.85	0.15	0.87	0.17	−0.66
Tbn5	13.5	4.7	2.8	0.68	2.8	0.60	0.17	0.84	0.27	0.81	0.13	0.85	0.14	−0.78
Tbn6	17.1	5.7	4.0	0.96	4.1	0.75	0.19	1.18	0.33	0.95	0.17	1.11	0.21	−0.74
Tbn7	1.2	0.6	0.4	0.06	0.3	0.05	0.02	0.09	0.02	0.07	0.01	0.08	0.01	−0.70
Tbn8	29.4	9.1	5.3	1.35	5.4	1.09	0.32	1.78	0.52	1.53	0.26	1.64	0.31	−0.79
Tbn9	49.7	16.9	10.9	2.74	11.6	2.45	0.64	3.36	0.88	2.74	0.41	2.75	0.46	−0.77
Tbn10	71.5	23.8	15.0	3.77	16.6	3.47	0.90	4.77	1.24	4.00	0.60	3.81	0.67	−0.79
Tbn11	87.1	28.5	14.5	4.16	18.0	3.90	0.93	5.47	1.42	4.88	0.73	4.81	0.80	−0.86
Tbn12	18.5	7.1	5.2	1.09	4.9	0.99	0.23	1.31	0.38	1.10	0.17	1.21	0.21	−0.72
Tbn13	38.1	13.9	8.0	1.95	8.5	1.77	0.49	2.51	0.67	2.12	0.30	1.92	0.30	−0.80
Tbn14	41.8	14.3	7.3	1.73	7.3	1.50	0.27	2.29	0.67	2.29	0.34	2.16	0.40	−0.82
Tbn15a	41.2	14.7	8.1	1.94	7.9	1.73	0.41	2.32	0.64	2.17	0.34	2.22	0.37	−0.80
Tbn15b	30.9	10.7	7.4	1.62	6.7	1.47	0.38	1.88	0.54	1.65	0.24	1.65	0.28	−0.72
Tbn16a	198.0	68.5	43.8	10.71	45.9	9.23	2.41	13.23	3.59	11.42	1.77	11.48	2.01	−0.77
Tbn16b	106.3	40.2	22.1	5.40	23.1	4.45	1.15	6.44	1.90	6.41	0.92	5.88	1.10	−0.81
Tbn17	42.5	18.1	18.2	3.24	14.0	2.66	0.69	3.33	0.85	2.66	0.39	2.51	0.42	−0.60
Deir1	8.2	3.2	2.0	0.44	1.9	0.40	0.10	0.64	0.17	0.48	0.07	0.48	0.08	−0.76
Deir2	102.9	37.7	20.3	5.19	23.5	5.10	1.42	7.07	2.02	6.69	0.93	6.29	1.03	−0.83
Deir3	40.5	16.0	12.7	2.69	10.9	2.25	0.61	2.83	0.75	2.45	0.35	2.39	0.39	−0.68
Deir4	16.1	6.6	5.2	1.00	4.5	0.96	0.25	1.13	0.31	0.93	0.14	0.92	0.16	−0.68
Deir5	5.8	3.5	3.2	0.55	2.3	0.44	0.12	0.52	0.14	0.39	0.06	0.42	0.06	−0.61
Deir6	23.1	7.6	5.6	1.20	5.1	1.08	0.17	1.50	0.40	1.30	0.20	1.32	0.24	−0.71
Deir7	21.8	7.8	4.6	1.04	4.8	0.91	0.24	1.25	0.33	1.09	0.16	1.07	0.19	−0.79
Deir8	29.2	9.9	4.4	1.16	5.2	0.97	0.28	1.52	0.48	1.60	0.22	1.59	0.27	−0.89
Deir9	2.5	1.1	0.9	0.11	0.5	0.12	0.02	0.17	0.03	0.11	0.02	0.12	0.02	−0.60
Deir10	16.4	5.7	3.7	0.75	3.2	0.61	0.19	0.99	0.30	0.87	0.14	0.88	0.17	−0.73
Deir11	15.9	5.0	2.4	0.61	2.4	0.56	0.14	0.80	0.27	0.86	0.12	0.78	0.13	−0.84
Deir12	36.9	12.0	5.4	1.48	6.6	1.10	0.34	2.05	0.58	1.95	0.29	1.88	0.33	−0.89
Deir13a	38.1	13.3	4.7	1.29	5.6	1.19	0.38	1.81	0.58	2.17	0.30	1.96	0.34	−0.95
Deir13b	1.7	0.6	0.6	0.08	0.3	0.05	0.02	0.09	0.02	0.06	0.01	0.07	0.01	−0.53
Deir14	14.8	5.7	5.2	0.95	4.1	0.77	0.20	1.07	0.27	0.91	0.13	0.81	0.14	−0.63
Deir15a	82.1	28.9	15.8	3.88	16.7	3.28	0.87	5.02	1.38	4.26	0.63	4.08	0.72	−0.81
Deir15b	88.5	28.1	12.4	3.88	17.3	3.58	0.93	5.15	1.50	4.85	0.71	4.76	0.84	−0.92
Deir15c	30.6	15.2	16.3	2.79	11.7	2.24	0.57	2.62	0.61	1.91	0.27	1.77	0.31	−0.57
Deir16	85.4	30.3	16.2	4.16	18.3	3.67	0.98	5.34	1.47	4.53	0.68	4.58	0.80	−0.83
Asad 1a	16.0	7.6	8.6	1.32	5.6	1.03	0.28	1.39	0.31	0.99	0.16	1.02	0.17	−0.54
Asad 1b	1.4	0.7	0.5	0.08	0.4	0.06	0.02	0.09	0.03	0.08	0.01	0.11	0.02	−0.69
Asad 2	32.0	10.8	8.3	1.81	7.6	1.50	0.48	2.07	0.53	1.69	0.26	1.63	0.31	−0.70
Asad 3	18.6	8.4	8.5	1.42	6.1	1.12	0.33	1.41	0.37	1.18	0.16	0.98	0.18	−0.59
Asad 5a	35.3	13.4	7.4	1.71	7.5	1.46	0.43	2.15	0.60	2.01	0.29	1.82	0.34	−0.80
Asad 5b	41.8	14.4	6.7	1.86	8.3	1.58	0.40	2.25	0.65	2.26	0.32	2.04	0.36	−0.88
Asad 6	13.0	5.2	3.4	0.71	2.9	0.69	0.15	0.75	0.22	0.72	0.10	0.69	0.14	−0.73
Asad 7	20.2	9.0	5.9	1.13	5.3	1.02	0.29	1.38	0.35	1.16	0.17	1.12	0.19	−0.74
Asad 8a	22.0	7.6	3.5	0.89	3.5	0.82	0.20	1.18	0.33	1.12	0.17	1.15	0.20	−0.85

Table 3 (continued)

NASC	Y	31.1 La	66.7 Ce	7.7 Pr	27.4 Nd	5.59 Sm	1.18 Eu	4.9 Gd	1.02 Ho	2.84 Er	0.48 Tm	3.06 Yb	0.46 Lu	Ce anomaly
Asad 8b	18.4	6.2	3.0	0.75	3.3	0.65	0.19	0.98	0.30	0.98	0.14	0.99	0.17	−0.85
Asad 9	19.5	6.3	2.6	0.72	3.1	0.65	0.17	0.92	0.30	1.00	0.15	0.97	0.16	−0.91
Asad 10	35.5	12.7	10.3	1.88	7.9	1.63	0.44	2.19	0.62	1.93	0.29	1.84	0.35	−0.65
Asad 11a	76.6	26.0	12.5	3.59	15.5	3.22	0.80	4.68	1.38	4.51	0.64	4.09	0.74	−0.87
Asad 11b	62.6	20.4	9.3	2.71	11.9	2.44	0.64	3.64	1.03	3.42	0.50	3.28	0.58	−0.89
Asad 12	48.9	17.4	9.6	2.56	11.3	2.23	0.62	3.20	0.97	3.07	0.44	2.97	0.52	−0.83
Zqb 1	59.9	20.1	11.3	2.91	11.7	2.59	0.70	3.60	1.03	3.31	0.47	3.35	0.57	−0.80
Zqb 2	21.3	10.8	7.5	1.43	6.0	1.27	0.26	1.50	0.39	1.28	0.18	1.07	0.21	−0.70
Zqb 3	11.0	6.4	6.4	0.98	4.3	0.84	0.20	1.00	0.21	0.65	0.10	0.70	0.11	−0.58
Zqb 4	42.5	16.8	8.6	2.16	9.4	1.89	0.49	2.74	0.66	2.22	0.36	2.21	0.38	−0.84
Zqb 5a	30.1	11.7	5.6	1.36	5.3	1.10	0.27	1.67	0.51	1.69	0.24	1.53	0.27	−0.83
Zqb 5b	28.2	9.8	4.6	1.16	5.6	0.89	0.25	1.55	0.46	1.37	0.22	1.49	0.27	−0.88
Zqb 6	26.3	10.0	8.6	1.47	6.2	1.25	0.30	1.68	0.43	1.43	0.22	1.41	0.26	−0.63
Zqb 7	41.6	14.5	8.4	1.91	8.6	1.72	0.52	2.42	0.69	2.16	0.31	1.91	0.33	−0.79
Zqb 8	50.4	16.7	7.0	2.28	9.7	2.09	0.55	2.91	0.86	2.78	0.41	2.55	0.48	−0.93
Av	37.4	13.4	8.1	1.91	8.2	1.67	0.44	2.36	0.66	2.12	0.32	2.06	0.36	−0.76
SW	170	57.1	7.85	8.6	37.5	7.37	1.82	10.5	3.46	11.9	1.86	13.2	2.45	−1.43

SW seawater analysis in ppm ($\times 10^{-7}$) for a sample obtained from 2000-m water depth in the Atlantic sector of the Southern Ocean (after Hathorne et al. 2012)

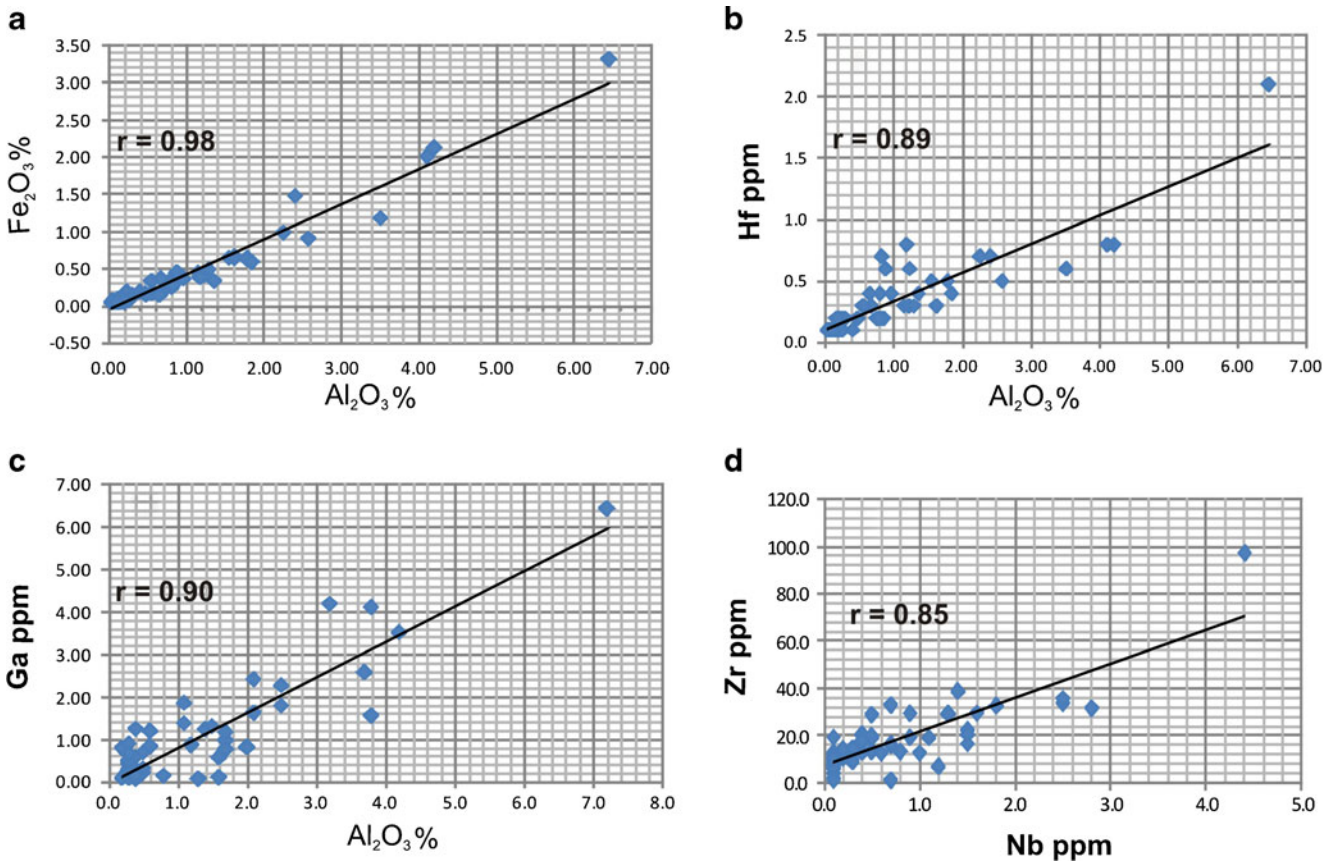

Fig. 5 Representative binary plots with the correlation coefficient "*r*" for some elements from the land-derived clay fraction, **a** Al_2O_3 and Fe_2O3, **b** Al_2O_3 and Hf, **c** Al_2O_3 and Ga, and **d** Zr and Nb. The *top samples at the end of all four lines* are extreme values. The plots are on the power of the samples, not on the clay fraction

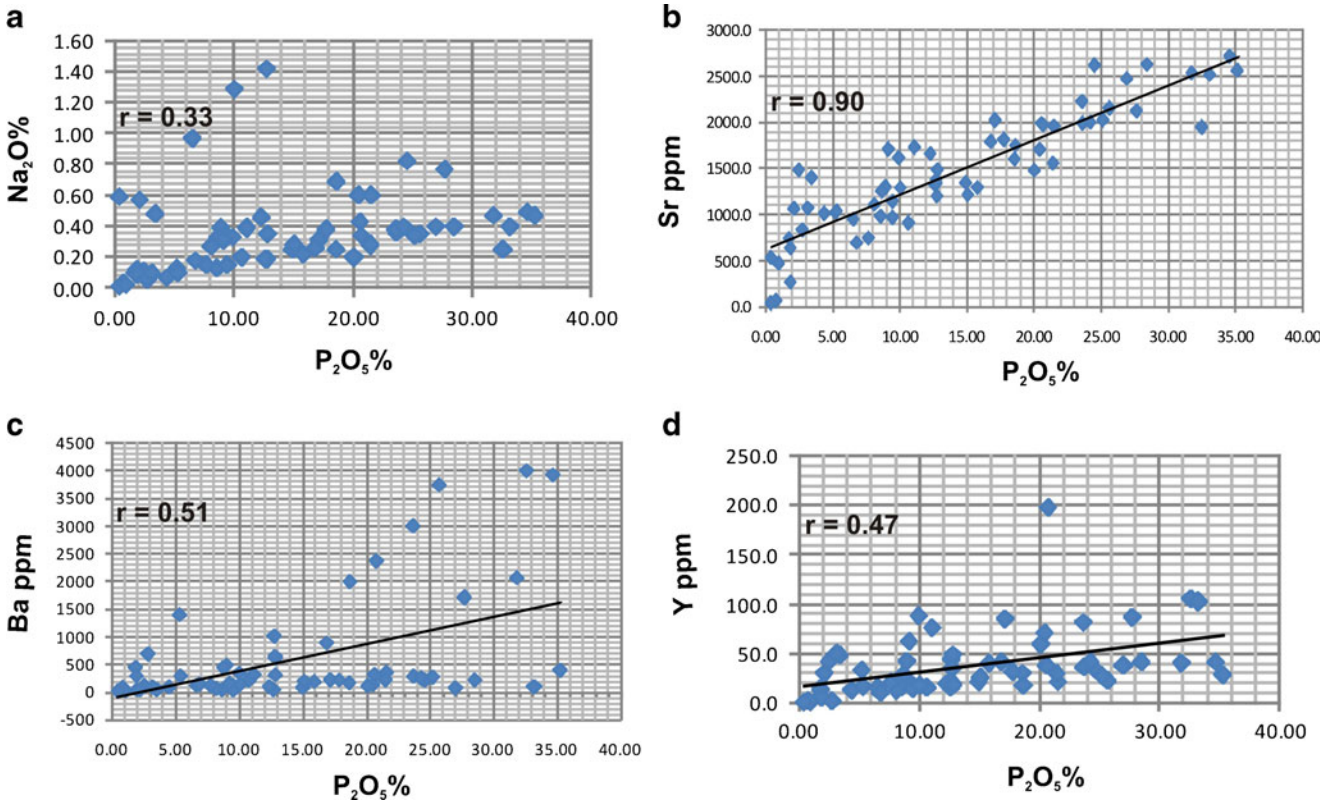

Fig. 6 Binary plots with "*r*" for the elements associated with CFA, **a** P_2O5 and Na_2O, the *upper left* few samples may indicate some addition of Na from groundwater; **b** P_2O5 and Sr; **c** P_2O5 and Ba, the *lower, horizontal sample* population represents carbonate and low-phosphate samples; and **d** P_2O5 and *Y*

removed from seawater, and consequently creates a negative Ce abundance in seawater and the sediments derived from it such as CFA, glauconite, and opal. The removed Ce^{4+} is, most probably, adsorbed on oxyhydroxides of Mn and Fe of the oceans, which may explain the positive Ce anomaly in, for example, Mn nodules on the ocean floor (e.g., Wright et al. 1987). Also, the REE in the seawater-derived sediments can be further fractionated through complexation especially with CO_3^{2-}, which leads to higher concentrations of the heavy REE relative to the light REE (e.g., Elderfield et al. 1981; Lee and Byrne 1993; Sholkovitz et al. 1994; Luo and Byrne 2004).

The REE patterns for the four sections of the studied samples, normalized to the North American shale composite (NASC), are shown in Fig. 9. Normalization is made by dividing each REE element in the studied sample by the respective element in NASC and recording the ratio. All the plots show a negative Ce anomaly and an enrichment of the heavy REE relative to the light elements, typical of the worldwide CFA pattern (e.g., Wildman and Haskin 1965; McArthur and Walsh 1984; Wright et al. 1987; Piper and Bau 2013). Among the other seawater-derived sediments such glauconite, biogenic carbonates, opal, and phillipsite, the CFA pattern is the closest to the REE pattern of seawater. This might indicate little or no changes to the CFA composition after formation (Dumoulin et al. 2011).

The CFA does not precipitate directly from seawater. There is a general agreement that phosphorites form under upwelling regimes (e.g., Glenn et al. 1994; Follmi 1996; Hathorne et al. 2012; Abed 2013; Alsenz et al. 2013; Föllmi et al. 2015). Upwelling currents spread deep, cold marine water on the sea surface of the relatively shallow continental platforms. Deep, cold water is usually rich in nutrients such Si and P, which are the basic food for the phytoplanktons, the lowest step in marine food chains which inhabit the photic zone or the upper 100–200 m of the seawater column. Thus, it increases the bioproductivity of the photoic zone which leads to higher content of organic-rich sediments in the upwelling area. Bacterial metabolism of organic matter liberates phosphate to pore water of the sediments in the upper millimeters or centimeters at the seafloor (e.g., Goldhammer et al. 2010; Bailey et al. 2013; Hiatt et al. 2015). It seems that the majority of the P in modern phosphorites is derived from organic matter (Froelich et al. 1982).This enhances the concentration of phosphates in the pore water and the precipitation of francolite. Pore water concentrations in modern Peru margin phosphogenic sediments range from 7 μmol/g up to extremes of 3700 μmol/g, which is due to bacterial breakdown of organic matter (Filippelli 1997). Amorphous calcium phosphate

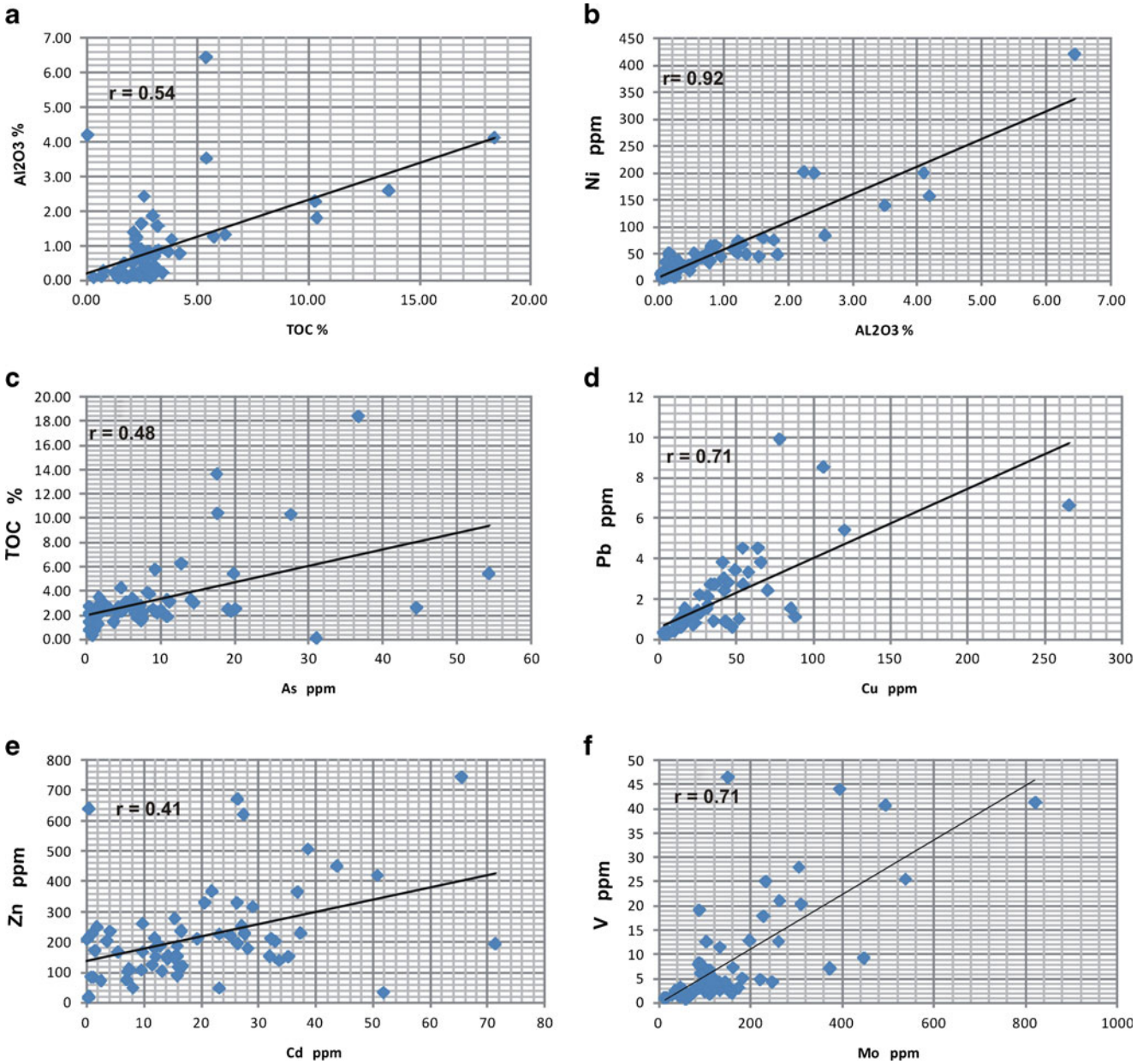

Fig. 7 Binary plots with "*r*" for the group of elements associated with the TOC and detrital clays. **a** Al_2O_3% and TOC%, **b** Al_2O_3% and Ni ppm, **c** TOC% and As ppm, **d** Pb ppm and Cu ppm, **e** Zn ppm and Cd ppm, and **f** V ppm and Mo ppm

precipitates first which crystallizes into francolite while the sediments are millimeters to centimeters below the seafloor. While still in contact with seawater, francolite uptakes many major and trace elements such as, Mg, Na, F, Sr, and REE (e.g., Arning et al. 2009).

Francolite precipitates either authigenically from the pore water solution after being enriched in PO_4 after shallow burial or diagenetically through the replacement of preexisting sediments by similarly enriched interstitial solutions (e.g., Glenn et al. 1994). The Al-Kora phosphorites are dominantly authigenic with very few foraminiferal tests seen phosphatized in only five thin sections. In these thin sections, phosphatized shells are present beside nonphosphatized ones (Fig. 10).

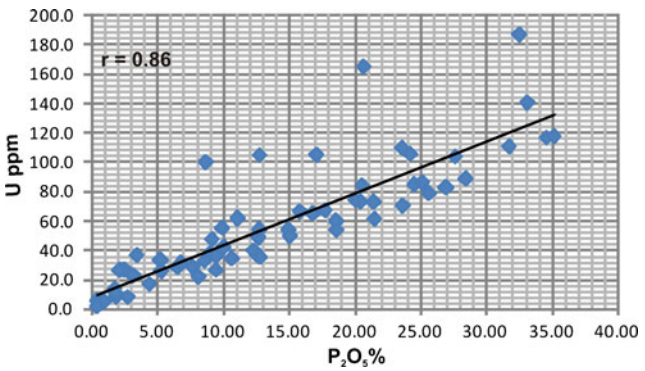

Fig. 8 A binary plot between uranium and the P_2O5 showing the highly significant, positive correlation coefficient between U and P_2O5

Table 4 Uranium contents (in ppm) in the Al-Kora phosphorites and the four sections compared with other Jordanian localities

Locality	Range	Mean
Eshidiyya	7–125	70
Central Jordan	34–190	105
Ruseifa	56–184	123
Al-Kora	1–186	58.4
Wadi Al-Arab	1.6–88.5	49.7
Dair Abu Sa'id	5.1–140.6	56.2
Tubna	5.6–186.8	69.8
Ziglab	22.9–105.3	59.5

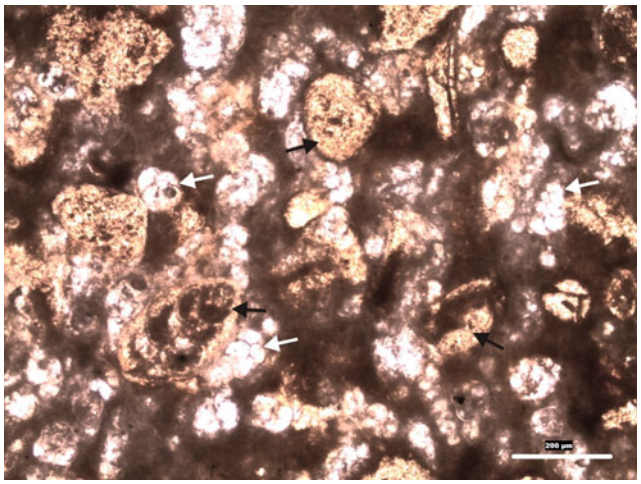

Fig. 10 A photomicrograph showing phosphatized foraminiferal test (*black arrows*) with nonphosphatized foraminiferal tests (*white arrows*), PPL

In most of the high-grade phosphorites, reworking and winnowing follow the precipitation of the CFA (e.g., Glenn et al. 1994; Riggs et al. 2000). Despite all these processes involved in the making of ancient phosphorites, the seawater signal in the REE pattern is kept very close to that of seawater, which is the case of the Al-Kora deposits.

All that said, there are some sporadic examples where the above described CFA pattern is different, e.g., the organic-rich, phosphatic shales of the Upper Carboniferous of midcontinent North America (Cruse et al. 2000). Here, the middle REE elements are enriched with no negative Ce anomaly except in the phosphate nodules where the REE patterns are similar to CFA described above. In our opinion, the CFA pattern, most probably, is obliterated by the abundant siliclastics in the shale samples, while it is kept clear in the phosphate nodules where the siliclastics are minor or absent.

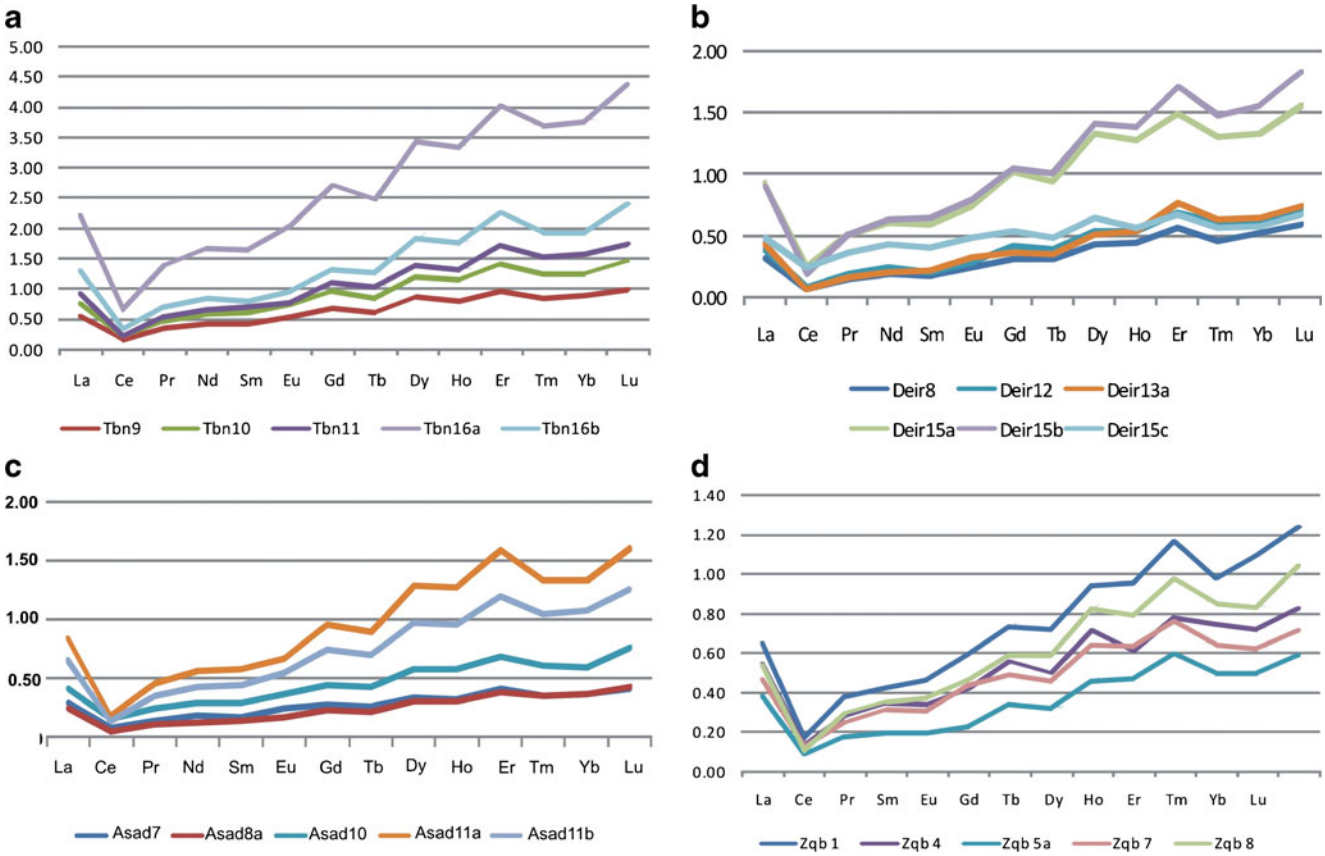

Fig. 9 Shale-normalized rare earth element patterns for samples representing the four measured sections, **a** Tubna, **b** Dair Abu Sa'id, **c** Wadi Al-Arab, and **d** Wadi Ziglab

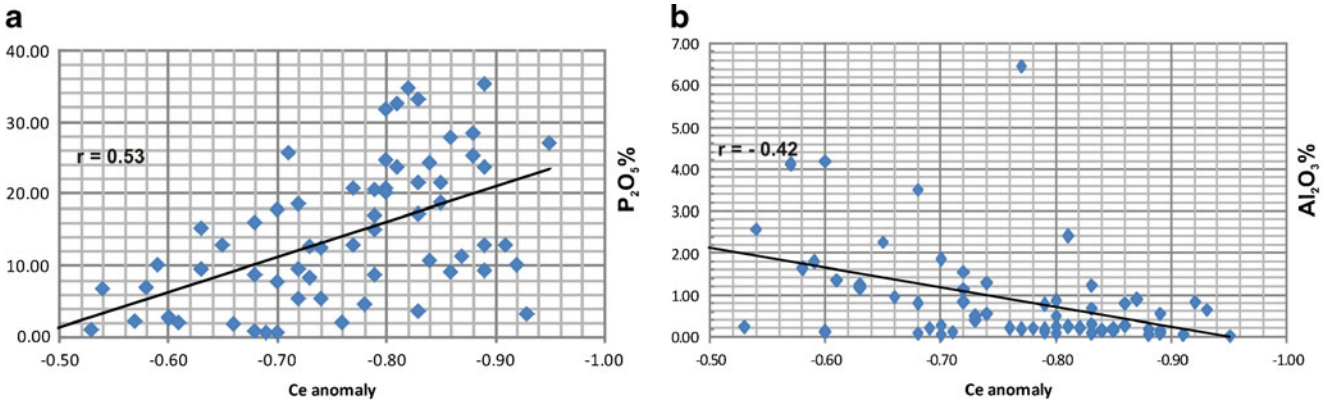

Fig. 11 The relationship between the negative Ce anomaly with **a** the seawater-derived CFA represented by P_2O5 (positive relation) and **b** the land-derived clays represented by Al_2O_3 (inverse relation)

Ce anomaly

The Ce anomaly is a prominent feature in the REE patterns. It is calculated in this section by the following equation (McArthur and Walsh 1984):

$$\text{Ce anomaly} = \log\left[\text{Ce}_n \Big/ (\text{La}_n + \text{Nd}_n)\right],$$

where "*n*" refers to the shale-normalized value. It is conducted on whole-rock powder, not on separated phosphate grains or vertebrate skeletal fragments.

The Ce anomaly in the samples investigated ranges between −0.53 and −0.95 with an average of −0.76. Samples with high P_2O_5% seem to have rather highly negative Ce anomalies. For example, samples Dair8, Dair13a, and Tbn11 have −0.89, −0.95, and −0.86 anomalies, with P_2O_5% 35.24, 26.99, and 27.72, respectively. However, there is a significant positive correlation coefficient (*r*) between the Ce anomaly and P_2O_5% equaling 0.57 (Fig. 11a). Also, there is a positive relationship between the less negative Ce anomaly samples with the higher Al_2O_3%. For example, the three samples with the least negative Ce anomalies, Dair13b, Dair13c, and Asad1a, −0.53, −0.54, and −0.57, have 1.04, 6.61, and 2.14 Al_2O_3%, respectively (see also Fig. 11b).

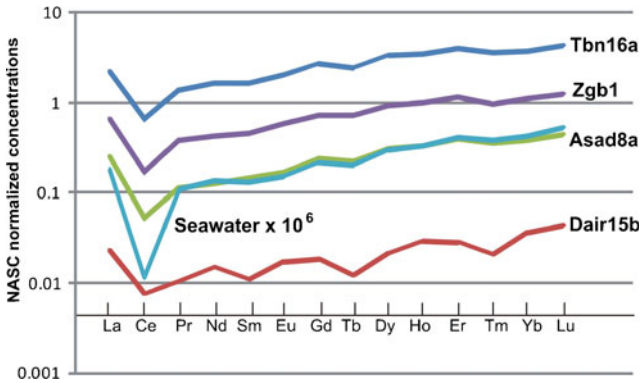

Fig. 12 Comparison of the Ce anomaly for four samples from the study area and a seawater sample obtained from 2000-m water depth in the Atlantic sector of the Southern Ocean (after Hathorne et al. 2012)

There are ample works on the geochemistry of REE and the Ce anomaly of the present-day ocean water. Examples include the Pacific Ocean (e.g., De Baar et al. 1985; Ruhlin and Owen 1986; Moller et al. 1992; Alibo and Nozaki 1999; Piper and Bau 2013), the Atlantic Ocean (e.g., De Baar et al. 1985; Hogdahl et al. 1968; Piper 1974; Hathorne et al. 2012; Piper and Bau 2013), and the Indian Ocean (e.g., Varghese 2004; Balaram et al. 2015). All these works, and many more, clearly indicated the presence of a negative Ce anomaly in present-day seawater and that the Ce anomaly increases with depth and increases with remoteness from the continental margins, because the CFA forms on the seafloor in the upper few millimeters to centimeters, i.e., in contact with the relatively deeper seawater, that would directly explains the negative Ce anomaly in the CFA. This is in agreement with the fact that ocean water at present is oxygenated. This led to the general agreement that the Ce anomaly can serve as an indicator to the redox potential of the seawater and the negative Ce anomaly records the oxic condition of the ocean water (e.g., De Baar et al. 1985; Wright et al. 1987; German and Elderfield 1990; Piepgras and Jacobsen 1992; Sholkovitz et al. 1994; Piper and Bau 2013).

Because the REE pattern and Ce anomaly in the CFA, as discussed above, are the closest to the REE of seawater, Wright et al. (1987) advocated the extrapolation of the use of the Ce anomaly in the CFA as a proxy to the redox potential in ancient seawater. Consequently, the negativity of the Ce anomaly of the CFA in ancient phosphorites has been successfully extrapolated backward, with some setbacks, to indicate the redox potential of the paleooceanic water masses and their relationship with the atmosphere O_2 abundance. Examples on the successful use of the CFA in this respect include the Late Cretaceous phosphorites of the Paris Basin and the Permian Phosphoria deposits (e.g., Jarvis 1984; Piper 2001).

The negative Ce anomalies of the Al-Kora phosphorite samples are compared to that of present-day ocean water (Table 3).The seawater sample was obtained from 2000-m water depth in the Atlantic sector of the Southern Ocean (Hathorne et al. 2012). Four samples are selected from the four studied localities and plotted and compared with seawater sample in Fig. 12. Figure 12 and Table 3 show that the Al-Kora phosphorite samples compare well with the seawater REE pattern and Ce anomaly. This would indicate that the deposition of Al-Kora phosphorites was from oxic seawater, or possibly from the oxygen minimum zone (OMZ), during the late Campanian-early Maastrichtian. Indeed, the ocean water masses were oxygenated during this period of the latest Late Cretaceous (e.g., Wang et al. 2011; Voigt et al. 2013). Also, the eastern Mediterranean phosphorites, including the Al-Kora deposits, as well as those of North Africa and parts of southern Europe, were deposited from the intense, westerly flowing, Tethyan circumglobal current (TCC). The TCC served as an upwelling current for those areas, spreading P and Si nutrients onto the surface platform water, thus enhancing bioproductivity and consequently the phosphorite formation (e.g., Follmi and Delamette 1991; Stampfli and Borrel 2002; Abed 2013).

Conclusions

1. Al-Kora phosphorites are dominantly granular (pelletal) phosphorite packstones/grainstones with minor laminated, in situ, pristine phosphorites. Because of the extreme rarity of phosphatized fossils, the Al-Kora deposits are considered authigenic in nature.
2. Based on the statistical correlations and factor analysis, the analyzed elements are distributed into (a) land-derived detrital clay group loaded with Al_2O_3, Fe_2O_3, TiO_2, K_2O, Cr, Ga, Hf, Nb, Rb, Th, and Zr, making less than 5 % of the of the samples analyzed; (b) marine- or seawater-derived phosphate-carbonate group loaded with P_2O_5, CaO, MgO, $N_{a2}O$, Ba, Sr, U, Y, and the 14 REEs, making the bulk of the samples; and (c) organic matter/detrital clay group loaded with Cr, Ni, Mo, Cu, Pb, As, Zn, and Sb.
3. Uranium resides in the CFA structure substituting for Ca. It averages 58.4 ppm with a range of 1–186 ppm. The average for the phosphate only samples is 101 ppm, which is comparable with other phosphorite deposits in Jordan. The low values are for the carbonate samples.
4. REE average is 44.5 ppm, too low to be of economic potential. Normalized REE patterns with NASC have a distinct negative Ce anomaly and enriched heavy REE relative to light REE, which is typical of seawater-derived minerals. This signal seems not have been affected by the diagenetic processes associated with the formation of the CFA.
5. The Ce anomaly averages −0.76 for all samples analyzed, being more negative for the phosphorite-only samples. This negative Ce anomaly confirms the oxygenated conditions of the Neo-Tethys Ocean water conditions at the time of deposition of Al-Kora phosphorites during the late Campanian-early Maastrichtian of the Late Cretaceous. Consequently, the CFA can be used as an indicator for the seawater paleoredox conditions.

Acknowledgments We would like to thank the Deanship of Scientific Research at the University of Jordan for financially supporting this work. The authors are grateful to the anonymous referees of the Arabian Journal of Geosciences for their ideas and comments which greatly improved the manuscript.

Appendix

Table 5 Structural carbonates (%) in the francolite using the pair-peak method

Sample no.	CO_3^{2-} %
Dair2	3.10 %
Dair3	3.0
Dair4	2.95
Dair6	3.0
Dair8	1.85
Dair10	4.5
Dair11	3.20
Dair12	2.90
Dair13b	3.30
Dair15a	1.80
Dair16	6.0

Guldbrandson (1970) for some samples from Dair Abu Sa'id section

Table 6 Fluoride contents in some samples of the study area

Sample no.	F %
Dair2	3.31
Dair3	1.52
Dair4	0.95
Dair6	2.87
Dair8	3.97
Dair10	1.13
Dair11	0.82
Dair12	3.13
Dair13b	0.31
Dair15a	3.21
Dair16	1.76

References

Abed AM (2011) Review of uranium in the Jordanian phosphorites: distribution, genesis and industry. Jordan J Earth Environ Sci 4: 35–45

Abed AM (2013) The eastern Mediterranean phosphorite giants: an interplay between tectonics and upwelling. Geo Arabia 18:67–94

Abed AM, Al-Agha MR (1989) Petrography, geochemistry and origin of the NW Jordan phosphorites. J Geol Soc Lond 146:499–506

Abed AM, Ashour M (1987) Petrography and age determination of the NW Jordan phosphorites. Dirasat 14:247–63

Abed AM, Kraishan GM (1991) Evidence for shallow marine origin of a "Monterey Formation type" chert-phosphorite-dolomite association: Amman Formation, Late Cretaceous, Central Jordan. Facies 24:25–38

Abed AM, Sadaqah R (1998) Role of Upper Cretaceous oyster buildups in the deposition and accumulation of high-grade phosphorites in central Jordan. J Sediment Res 68:1009–1020

Abed AM, Saffarini GA, Sadaqah RM (2014) Spatial distribution of uranium and vanadium in the upper phosphorite member in Eshidiyya basin, southern Jordan. Arabian J Geosciences (Springer) 7(1):253–271. doi:10.1007/s12517-013-0837-1

Abella SR, Zimmer BW (2007) Estimating organic carbon from loss-on-ignition in northern Arizona forest soils. Am J Soil Sci Soc 71:545–550

Al-Bassam KS (2007) Mineral resources of western Iraq. In The Geology of Iraqi Western Desert. Iraqi Bulletin of Geology and Mining, Special Issue 3, 145–168.

Alibo DS, Nozaki Y (1999) Rare earth elements in seawater: particle association, shale-normalization, and Ce oxidation. Geochim Cosmochim Acta 63:363–372

Al-Kuisi M Abed AM Mashal K and Saffarini G (2015) Hydrogeochemistry of groundwater from karstic limestone aquifer highlighting arsenic contamination—case study from Jordan. Arabian Journal of Geosciences. doi: 10.1007/s12517-015-1919-z

Alsenz H, Regnery J, Ashckenazi-Polivoda S, Meilijson A, Ron-Yankovich L, Abramovich S, Illner P, Almogi-Labin A, Feinstein S, Berner Z, Püttmann W (2013) Sea surface temperature record of a Late Cretaceous tropical southern Tethys upwelling system. Palaeogeogr Palaeoclimatol Palaeoecol 392:350–358

Altschuler ZS (1980) The geochemistry of trace elements in marine phosphorites, Part 2: Characteristics, abundances and enrichment. SEPM Spec Publ 29:19–30

Arning ET, Birgel D, Brunner B, Peckmann J (2009) Bacterial formation of phosphatic laminites off Peru. Geobiology 7:295–307

Bailey JV, Corsetti FA, Greene SE, Crosby CH, Liu P, Orphan VJ (2013) Filamentous sulfur bacteria preserved in modern and ancient phosphatic sediments: implications for the role of oxygen and bacteria in phosphogenesis. Geobiology 11:397–405

Balaram V, Roy P, Subramanyam KSV, Durai L, Ram Moham M, Satayanarayanan M, Sawant SS, Kalyan Kamal SS, Vani K (2015) REE geochemistry from Afanasy-Nikitin Seamount in north central Indian Ocean by high resolution inductively coupled plasma mass spectrometry. Indian J Geo-Marine Sci 44

Barghouthi Z, Amereih S (2012) Spectrophotometric determination of fluoride in drinking water using aluminium complexes of triphenylmethane dyes. Am J Anal Chem 3:651–655

Bender F (1974) Geology of Jordan. Borntraeger, Berlin, p 196

Bentor YK (1980) Phosphorites: the unsolved problems. *Marine phosphorites* (ed Bentor, Y.K.), Society of Economic Paleontologists and Mineralogists, Special Publications 29, 3–18

Brownlow AH (1996) Geochemistry, 2nd edn. Prentice Hall, New Jersey

Burdon DJ (1959) Handbook of the geology of Jordan. Government of Jordan, Amman, p 82

Capetta H, Pfeil F, Schmidt-Kittler N, Martini E (1996) New biostratigraphic data on the marine Upper Cretaceous and Paleogene of Jordan. Unpublished report by the Jordan Phosphate Mining Company, Amman

Cruse AM, Lyons TW, kidder DL (2000) Rare-earth element behavior in phosphates and organic-rich host shales: an example from the Upper Carboniferous of midcontinent North America. SEPM Spec Publ 66:445–453

De Baar D, Bacon D, Brewer MP, Bruland PG (1985) Rare earth elements in the Pacific and Atlantic Oceans. Geochim Cosmochim Acta 49: 1943–1959

Dumoulin JA Slack JF Whalen MT and Harris AG (2011) Depositional eetting and geochemistry of phosphorites and metalliferous black shales in the Carboniferous-Permian Lisburne Group, Northern Alaska. US Geological Survey Professional Paper 1776.

Elderfield H, Hawkesworth CJ, Greaves MJ, Calvert SE (1981) Rare earth element geochemistry of oceanic ferromanganese nodules and associated sediments. Geochim Cosmochim Acta 45:513–528

El-Hiyari M (1985) The geology of Jabal Al-Mutarammil, Map sheets No 3252, III. National Mapping Project, Bulletin 1, Natural Resources Authority, Amman

Filippelli GM (1997) Controls on phosphorus concentration and accumulation in oceanic sediments. Mar Geol 139:231–240

Flügel E (2004) Microfacies of carbonate rocks. Springer, Berlin

Follmi KB (1996) The phosphorus cycle, phosphogenesis and marine phosphate-rich deposits. Earth Sci Rev 40:55–124

Follmi KB, Delamette M (1991) Model simulation of mid-Cretaceous ocean circulation: technical comments. Science 251:94–95

Föllmi KB, Hofmann H, Chiaradia M, de Kaenel E, Frijia G, Parente M (2015) Miocene phosphate-rich sediments in Salento (southern Italy). Sediment Geol 327:55–71

Froelich PN, Bender ML, Luedtke NA, Heath GR, DeVries T (1982) The marine phosphorus cycle. Am J Sci 282:474–511

German CR, Elderfield H (1990) Application of the Ce anomaly as a paleoredox indicator: the ground rules. Paleoceanography 5:823–833

Glenn CR, Follmi KB, Riggs SR, Baturin GN, Grimm KA, Trappe J, Abed AM, Galli-Oliver C, Garrison RE, Ilyin AV, Jehl C, Rohrlich V, Sadaqah R, Schidlowski M, Sheldon R, Siegmund H (1994) Phosphorus and phosphorites: sedimentology and environments of formation. Eclogae Geol Helv 87:747–788

Goldhammer T, Brüchert V, Ferdelman TG, Zabel M (2010) Microbial sequestration of phosphorus in anoxic upwelling sediments. Nat Geosci 3:557–561

Gulbrandson RA (1970) Relation of carbon dioxide content of apatite of the Phosphoria Formation to regional facies. US Geol Surv Prof Paper 700B:B9–B13

Hamam KA (1977) Forminifera from the Maastrichtian bearing strata of Al-Hisa, Jordan. J Foraminifer Res 7:34–43

Hathorne EC, Haley B, Stichel T, Grasse P, Zieringer M, Frank M (2012) Online preconcentration ICP-MS analysis of rare earth elements in seawater. Geochem Geophys Geosyst 13:Q01020. doi:10.1029/2011GC003907

Hiatt EE, Pufahl PK, Edwards CT (2015) Sedimentary phosphate and associated fossil bacteria in a Paleoproterozoic tidal flat in the 1.85 Ga Michigamme Formation, Michigan, USA. Sediment Geol 319:24–39

Hogdahl T, Melson S, Bowen V (1968) Neutron activation analysis of lanthanide elements in seawater. Adv Chem Ser 73:308–325

Jacobs International (1992) Unpublished report, Al-Jalamid Phosphate Project, v. 2, Geology and Reserves, for the Saudi Arabian Deputy Ministry for Mineral Resources.

Jarvis I (1984) Rare earth element geochemistry of late cretaceous chalks and phosphorites from northern France. Geol Surv India Spec Publ 17:179–190

Jasinski SM (2011) Phosphate rock. In Mineral Commodity Summaries 2011, USGS, United States Government Printing Office, Washington, D.C.

JMPC (2013) Jordan Phosphate Mines Company annual report

Krauskopf K, Bird D (1995) Introduction to geochemistry, 3rd edn. McGraw Hill, Boston

Lee JH, Byrne RH (1993) Complexation of trivalent rare earth elements (Ce, Eu, Gd, Tb, Yb) by carbonate. Geochim Cosmochim Acta 57: 295–302

Lucas J and Prevot-Lucas L (1995) Tethyan phosphates and bioproductites. In A.E.M. Nairn and F.G. Stehli (Eds.), The Ocean Basins and Margins-The Tethys Ocean. Plenum Press, 8, p. 367–391

Luo YR, Byrne RH (2004) Carbonate complexation of yttrium and the rare earth elements in natural waters. Geochim Cosmochim Acta 68: 691–699

Masri M (1963) Unpublished report on the geology of the Amman-Zerqa Area. Central Water Authority, Amman

McArthur JM, Walsh JN (1984) Rare earth elements geochemistry in phosphorites. Chem Geol 47:191–220

McClellan GH (1980) Mineralogy of carbonate-fluorapatite. J Geol Soc London 137:675–681

McClellan GH and Kauvenbergh SJV (1990). Mineralogy of sedimentary apatite. In : A. J. G. Notholt and I. Jarvis (Eds.) Phosphorite Research and Development. Geol. Soc. London Spec. Publ., 52, 23–31.

McClellnn GH, Lehr JR (1969) Crystal-chemical investigation of natural apatites. Am Mineral 54:1374–1391

Mckelvey VE, Strobell JD, Slaughter AI (1986) The vanadiferous zone of the Phosphoria Formation in western Wyoming and southern Idaho, 1465. U. S. Geol. Surv. Prof. Paper, Alexandria, p 27

Mikbel S, Abed AM (1985) Discovery of large phosphate deposits in NW Jordan. Dirasat 12:125–124

Moller P, Dulski P, Luck J (1992) Determination of rare earth elements in seawater by inductively coupled pIasma-mass spectrometry. Spectrochim Acta 478:1379–1387

Nathan Y (1984) The mineralogy and geochemistry of phosphorites. In: Nriagu JO, Moore PO (eds) Phosphate minerals. Springer, Berlin, pp 275–291

Notholt AJ Sheldon RP and Davidson DF (1989) Phosphate deposits of the world, v. 2, Phosphate Rock Resources. Cambridge University Press.

Piepgras DJ, Jacobsen SB (1992) The behavior of rare earth elements in seawater: precise determination of variations in the North Pacific water column. Geochim Cosmochim Acta 56:1851–1862

Piper DZ (1974) Rare earth elements in the sedimentary cycle. Chem Geol 14:285–304

Piper DZ (2001) Marine chemistry of the Permian Phosphoria formation and basin, Southeast Idaho. Econ Geol 96:599–620

Piper DZ, Bau M (2013) Normalized rare earth elements in water, sediments, and wine: identifying sources and environmental redox conditions. Am J Anal Chem 4:69–83

Powell J (1989) Stratigraphy and sedimentation of the Phanerozoic rocks in central and south Jordan, part B: Kurnub, Ajlun and Belqa Groups, Geology Directorate Bulletin, 11. Natural Resources Authority of Jordan, Amman

Powell J, Moh'd BK (2011) Evolution of Cretaceous to Eocene alluvial and carbonate platform sequences in central and south Jordan. Geo Arabia 16(4):29–82

Powell J, Moh'd BK (2012) Early diagenesis of chalk-chert-phosphorite hardgrounds (Coniacian-Campanian) of central Jordan; implications for sedimentation on a Late Cretaceous shallow pelagic ramp. Geo Arabia 17(4):17–38

Prevot L (1990) Geochemistry, petrography, genesis of Cretaceous-Eocene phosphorites; the Ganntour deposit (Morocco): a type example. Societe Geologique de France, Paris, p 232

Prevot L, Lucas J (1980) Behaviour of some trace elements in phosphatic sedimentary formations. In: Bentor YK (ed) Marine phosphorites, vol 29, SEPM Special Publ., pp 31–41

Pufahl PK, Grimm KA, Abed AM, Sadaqah R (2003) Upper Cretaceous (Campanian) phosphorites in Jordan: implications for the formation of a south Tethyan phosphorite giant. Sediment Geol 161:175–205

Riddler PK, Van Eck M, Farasani AM (1989) The phosphorite deposits of the Sirhan-Turayf region, northern Saudi Arabia. In: Notholt AJG, Sheldon RP, Davidson DF (eds) Phosphate deposits of the world, vol 2. Cambridge University Press, Phosphate Rock Resources, pp 332–339

Riggs S, Snyder SW, Ames D, Stille P (2000) Chrono-stratigraphy of upper Cenozoic phosphorites on the North Carolina continental margin and the oceanographic implications for phosphogenesis. SEPM Spec Publ 66:369–385

Ruhlin DE, Owen RM (1986) The rare earth element geochemistry of hydrothermal sediments from the East Pacific Rise: examination of a seawater scavenging mechanism. Geochim Cosmochim Acta 50: 393400

Sadaqah RM (2000) Phosphogenesis, geochemistry, stable isotopes and depositional sequence of the Upper Cretaceous phosphorite formation in Jordan. Unpubl PhD thesis, Univ of Jordan, Amman, 257

Sharland PR, Higher R, Casey DM, Davies RB, Hall SH, Heward AP, Horbury AD, Simmons MD (2001) Arabian plate sequence stratigraphy. GeoArabia Special Publication 2. Gulf PetroLink, Bahrain, p 371

Sholkovitz ER, Landing WM, Lewis BL (1994) Ocean particle chemistry: the fractionation of the rare earth elements suspended particle and seawater. Geochim Cosmochim Acta 58:1567–1579

Slansky M (1986) Geology of sedimentary phosphates. Elsevier, Amsterdam

Stampfli GM, Borrel H (2002) A plate tectonic model for the Paleozoic and Mesozoic constrained by dynamic plate boundaries and restored synthetic oceanic isochrones. Earth Planet Sci Lett 196:17–33

Sun H, Nelson M, Chen F, Husch J (2009) Direct spectrophotometric fluoride determination. Can J Soil Sci 89(5):603–610

Van Kauwenbergh SJ (2010) World phosphate rock reserves and resources. International Fertilizer Development Center (IFDC), Technical Bulletin 75, Muscle Shoals, Alabama.

Varghese S (2004) Geochemistry of rare earth elements and trace metals along the western continental shelf of India. Un published Ph. D thesis, Cochin University of Science and Technology, Kochi

Voigt S, Jung C, Friedrich O, Frank M, Teschner C, Hoffmann J (2013) Tectonically restricted deep-ocean circulation at the end of the Cretaceous greenhouse. Earth Planet Sci Lett 369–370: 169–177

Wang C, Hu X, Huang Y, Wagreich M, Scott R, Hay W (2011) Cretaceous oceanic red beds as possible consequence of oceanic anoxic events. Sed Geol 235:27–37

Weaver C, Polland L (1975) The chemistry of clay minerals. Elsevier Scientific Publication, Amsterdam

White WM (1997) Geochemistry. Cornell University, USA. <http://www.geo.cornell.edu/geology/classes/geo455/Chapters.HTML>.

Wildman TR, Haskin L (1965) Rare-earth elements in ocean sediments. J Geophys Res 70:2905–2911

Wright J, Schrader H, Holster W (1987) Paleoredox variations in ancient oceans recorded by rare earth elements in fossil apatite. Geochim Cosmochim Acta 51:631–644

Yamamura SS, Wade MA, Sikes JH (1962) Direct spectrophotometric fluoride determination. Anal Chem 34(10):1308–1312